Realistic Field Theories on Submanifolds of Compact Extra Dimensions

Eugene Amaru Mirabelli

Ph.D. Thesis, Stanford University, Stanford, CA 94309
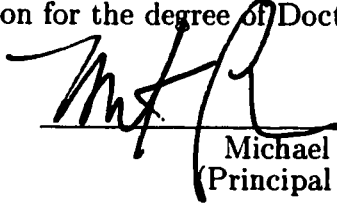
REALISTIC FIELD THEORIES
ON SUBMANIFOLDS OF
COMPACT EXTRA DIMENSIONS

Eugene Amaru Mirabelli

December 1999

I certify that I have read this dissertation and that in my opinion it is fully adequate, in scope and quality, as a dissertation for the degree of Doctor of Philosophy.

Michael Peskin
(Principal Adviser)

I certify that I have read this dissertation and that in my opinion it is fully adequate, in scope and quality, as a dissertation for the degree of Doctor of Philosophy.

Savas Dimopoulos

I certify that I have read this dissertation and that in my opinion it is fully adequate, in scope and quality, as a dissertation for the degree of Doctor of Philosophy.

Lance Dixon

Approved for the University Committee on Graduate Studies:

iii

Preface

This thesis discusses various physical scenarios in which the particles of the standard model are trapped on a 4-dimensional manifold in a higher-dimensional space.

First, we study a model suggested by Hořava and Witten which resolves the discrepancy between the gravitational and gauge couplings at the fundamental scale of string theory. In their model there is a scale at which space is effectively 5-dimensional and the standard model particles, confined to one 4-dimensional boundary, feel the effects of soft supersymmetry breaking in a hidden sector located on the other boundary. We use auxiliary fields to derive supersymmetric couplings between boundary matter and bulk super-Yang-Mills fields. We then display two methods of supersymmetry breaking and compute the Casimir energy of the system.

We then discuss Arkani-Hamed, Dimopoulos, and Dvali's solution to the hierarchy problem. In their model, the standard model particles live on a 4-dimensional membrane in a space with large ($\approx$ mm) extra dimensions. We calculate the cross section to emit gravitons into the extra dimensions. Current collider constraints on these cross sections demand a compactification scale less than 0.47 mm, while future experiments could push that constraint to .012 millimeters.

Finally, there is an exploration of Arkani-Hamed and Schmaltz's mechanism for generating hierarchies among Yukawa couplings through the relative displacement of the locations of the standard model fields within a 4-dimensional membrane in a higher-dimensional space. We find only one configuration of displacements consistent with experiment, with a prediction for the strange quark mass $m_s^{\overline{MS}}(2\ GeV) \approx$ $(1.19) \times (V_{ub}V_{cb}/V_{us})^{1/2} \times m_b^{\overline{MS}}(m_b) \approx 120\ MeV$.

Acknowledgments

This is dedicated to Dad, Mom, Francesca and Gabriella.

Contents

List of Figures

Chapter 1

Introduction

In this thesis, we study various physical models which assume the existence of spatial dimensions beyond the familiar three. While everyday observation suggests only three dimensions, there is no shortage of potential explanations for how extra dimensions could have escaped our detection for so long. For instance, the extra dimensions could be compact, curled into a microscopic volume so that you can never move far in the extra dimension without ending up back where you started. Or, the elements of everyday experience could be trapped on a three-dimensional membrane floating in a higher dimensional space. The models studied in this thesis each use both of these mechanisms in tandem (see figure 1.1), with electrons, photons, quarks, and the like being confined to a three-dimensional membrane that sits in a space with compact extra dimensions. Gravitons (and perhaps other new types of particles) could travel beyond the three-dimensional membrane, so we can feel the effects of the higher-dimensional space, but because the extra dimensions are compactified on a small scale, the effects are subtle.

1.1 Force Unification from Extra Dimensions

Around the turn of the century, physicists hoped to follow up the unification of electric and magnetic forces with a unification of electromagnetism with the other long-range force: gravity. Kaluza-Klein theory provided such a unification, but it

compactified

confined to sub-manifold

confined to sub-manifold in compact dimension
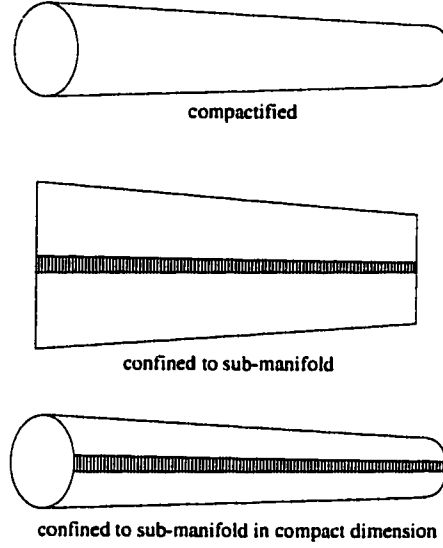
Figure 1.1: Hiding extra dimensions.

required the introduction of an extra dimension. The theory could be extended to include the strong and weak forces, but it could not be made realistic, as it could not accommodate light charged fields or charged matter with a definite helicity, which are present in the real world.

About thirty years ago, string-theory models were found which not only unified gravitational and gauge force phenomena, but also unified fermion matter fields and bosonic force fields in terms of different excitations of a single object: the supersymmetric string. However, at the quantum level, the theory required extra dimensions for consistency. These extra dimensions created new tools for model building–the non-observation of these dimensions demanded that they be wrapped up into a small compact manifold, and different compactification choices led to different low energy models, with different types of matter and forces.

The $E_8 \times E_8$ heterotic variant of string theory, suitably compactified on a Calabi-Yau manifold, appeared particularly promising, as it could contain the observed three generations of matter appropriately charged under standard model gauge forces (or

super-grand-unified generalizations thereof). It even suggested a mechanism for low-energy supersymmetry breaking—standard model matter would be charged under one E_8, whose sub-group E_6 had just the right complexity to contain the standard model forces, while the other E_8 could become strongly coupled at low energies, leading to gaugino condensation and supersymmetry breaking, which could then be mediated to standard model particles via gravitational forces.

However, the string paradigm was not without problems. One of the few clues that current experimental results provide for physics beyond the standard model is that the interaction strengths of the strong, electroweak isospin, and electroweak hypercharge forces, directly measured at distance scales as small as 10^{-18} meters, all extrapolate to a single strength at the much smaller distance scale $\ell_{GUT} = 10^{-32}$ meters (if the extrapolation is calculated under the assumption of electroweak-scale supersymmetry). This suggests that physics beyond the standard model can be described by a super-symmetric "grand unified" theory, in which the strong and electroweak forces derive from a single force at short distance scales of order ℓ_{GUT}. The most straightforward weakly-coupled string theory models predict the existence of effective grand unified theories, but they generally predict that the forces unify at a length scale roughly thirty times smaller than the extrapolated unification scale ℓ_{GUT}. It is remarkable that the string theory prediction for the unification scale should be so close to the observed unification scale, but the discrepancy is large and robust enough to demand explanation. Another problem with the string paradigm was that weakly-coupled string models seemed to generically suffer from a "runaway modulus" problem in which the scalar field which controls the interaction strength of the theory would relax so as to move the theory from weak coupling towards zero coupling. This was considered an argument that realistic string theories must not be weakly coupled, but at the time string models were defined solely in terms of a perturbative weak coupling expansion, and nonperturbative string effects could not be discussed.

With the recent "revolution" in nonperturbative string/M theory, clues about the behavior of string/M theory at large coupling emerged. Hořava and Witten demonstrated that the low energy physics of strongly coupled *ten*-dimensional $E_8 \times E_8$ heterotic string theory was mimicked by weakly coupled *eleven*-dimensional supergravity

interacting with two ten-dimensional E_8 gauge theories, with the eleventh dimension compactified on the orbifold S^1/Z_2 (i.e. a line segment) and the ten-dimensional E_8 gauge theories localized in the eleventh dimension at the orbifold fixed points (i.e. the line segment endpoints). It appears that strongly coupled string theory "grows" another dimension!

In addition to providing a strongly coupled model, Witten has shown that this theory, further compactified on a Calabi-Yau manifold and given appropriately chosen values of the string coupling and the line segment size, can remove the factor of thirty discrepancy between the predicted and observed gauge force unification scales. Briefly put, in the weakly coupled model, at low energies, the universe could be described by a four-dimensional effective field theory, with the standard model interaction strengths unifying as mentioned earlier. If the gauge and gravitational forces both experience some extra dimensions at distances smaller than some compactification scale, they both have similarly altered extrapolations to smaller distances, so that the gauge forces still unify with each other at some particular scale, and they still do not unify with the gravitational force at that scale. But if, as in the strongly coupled model, there is a scale at which gravity experiences a new dimension but the gauge forces do not (being stuck on the endpoints), then the extrapolation of the gravitational force will be altered at distances smaller than this scale while the behavior of the gauge forces is not. The size of the line segment can then be tailored so that the altered gravitational extrapolation meets up with the gauge coupling strength at the length scale ℓ_{GUT}.

When the line segment size is tailored in this fashion, it is larger than the Calabi-Yau, creating a length regime between these scales in which the theory can be treated as a five-dimensional supersymmetric effective field theory with two four-dimensional boundaries at the Z_2 fixed points. Thus realistic string-derived models may be studied in the context of a five-dimensional effective field theory coupled to two four-dimensional effective field theories at the boundaries of the fifth dimension. In this context, supersymmetry breaking in the "other" E_8 is supersymmetry breaking on the "other" boundary of the extra dimension. Low-energy supersymmetry breaking,

which may be observed at near-future collider experiments, would thus involve extra-dimensional physics in an essential way. The possibility that the distinctive nature of such a model might lead to distinctive signatures in low-energy physics makes this system worth investigating.

In chapter 2, we study the dynamics of a "toy model" inspired by such a system. We examine the dynamics of a five-dimensional flat-space gauge supermultiplet (with Z_2 projected boundary conditions) coupled to four-dimensional boundary N=1 chiral supermultiplets and devise an algorithm for deriving general couplings between boundary matter and bulk super-Yang-Mills fields through the use of auxiliary fields. We explain the appearance of certain formally divergent terms in the supersymmetry-invariant Lagrangian, and then show that these divergences do not interfere with standard perturbative calculations, which we use to display two scenarios exhibiting the transmission of supersymmetry breaking effects from one boundary to the other. After supersymmetry breaking, the Casimir vacuum energy of the system can be nonzero, and in a model with gravity, the minimization of this energy would fix the size of the extra dimension. We compute the vacuum energy in the presence of supersymmetry breaking. This work was originally presented in [1], and chapter 2 is based closely on that publication.

1.2 Extra Dimensions and Hierarchies

Physical models with extra dimensions have traditionally allowed all the fields of the model to experience the same number of extra dimensions, but with recent results in nonperturbative string/M theory involving quantum fields confined to membranes and "D-branes" as well as degrees-of-freedom in higher dimensions, there has been increasing interest in models in which different numbers of extra dimensions are accessible to different fields. As such theories were, until recently, largely unexplored, they offer many new possibilities for exotic solutions to familiar theoretical problems, such as the electroweak hierarchy problem and the flavor problem described below.

In the contemporary understanding of quantum field theory, the special form of

the standard model Lagrangian is understood to be derivable as the low energy limit of a rather generic effective quantum field theory defined at a high energy scale such as the Planck scale. Whatever the correct fundamental physical theory is, it can be approximated by local quantum field theories at low energies. Making no assumptions about the fundamental theory, one can write down a generic effective field theory for a collection of fields at the Planck scale by including all possible Lagrangian terms allowed by the gauge symmetries of the theory.

When these Lagrangian terms are renormalized to an effective theory at the weak scale, most terms are suppressed by powers of M_{weak}/M_{Planck}, with the remaining dominant terms being the familiar renormalizable ones: canonical gauge-covariant kinetic terms, mass terms, Yukawa couplings, and cubic and quadratic scalar self-interactions. Mass terms allowed by gauge symmetries (i.e. scalar, Majorana, and Dirac masses) would generically be roughly of order M_{Planck} and fields with these masses could be neglected in the weak-scale theory. Then the only fields visible at the weak scale should be gauge fields and fermions charged under chiral gauge symmetries.

The most prominent exceptions to this understanding are the cosmological constant (i.e. the vacuum energy density) and the Higgs field mass and expectation value. In the aforementioned framework it is difficult to understand why these should not all have magnitudes of roughly the Planck mass raised to the appropriate power. Instead, the observed energy scale of electroweak breaking as set by the Higgs expectation value is observed to be approximately 10^{-17} times the Planck mass, and the cosmological constant, which is expressed in units of mass raised to the fourth power, is measured to be less than 10^{-116} times the fourth power of the Planck mass.

Additionally, there is a less extreme problem with the sizes of the first and second generation fermion masses. Given that the electroweak symmetry which prevents the standard model fermions from having masses is broken at an energy scale of roughly 100 GeV, we would expect the fermion masses to be roughly 100 GeV as well, corresponding to dimensionless Yukawa couplings which are $O(1)$. Instead, we find a hierarchical spectrum of Yukawa couplings among the different flavors of quarks, and while the top quark Yukawa is roughly equal to one, the up quark coupling is

about fifty thousand times smaller.

While the cosmological constant problem is still unsolved, tentative theoretical resolutions of the electroweak "hierarchy problem" exist based on low-energy super-symmetry and technicolor models, and various flavor models exist which could explain the Yukawa structure.

Arkani-Hamed, Dimopoulos, and Dvali propose a more radical solution[1] to the hierarchy problem in a model which confines non-gravitational standard model fields to a membrane floating in a higher-dimensional space. They propose that the funda-mental scale of quantum gravity *is* the weak scale, and that the observed weakness of the gravitational force relative to the other forces is a result of the spreading of the graviton wavefunction into extra dimensions that the fields of the standard model cannot enter. This is similar to Witten's mechanism for achieving gauge and gravita-tional unification described in section 1.1, except that the size of the extra dimensions are tailored to make the gravitational interaction $O(1)$ at an energy of 1 TeV rather than making it of order α_{GUT} at 10^{13} TeV.

To sufficiently reduce the potency of the gravitational force on the four dimensional membrane, the compactification scale of the extra dimensions must be quite large— as large as a millimeter if there are only two extra dimensions. This is quite a change from traditional string/M models which assume extra dimensions to have a compactification scale on the order of the Planck, string, or grand-unification length scales (and thus safely hidden from experimental resolution at terrestrial energies). Models with such large extra dimensions suggest the exciting possibility that bizarre physics involving Kaluza-Klein modes, string excitations, and quantum gravity effects should be experimentally accessible in the near future.

Amazingly enough, such large extra dimensions are not already ruled out by cur-rent gravitational experiments (which have not probed much below a millimeter), nor are they ruled out by order-of-magnitude estimates of corrections to standard model particle physics experiments, as long as the extra-dimensional "thickness" of

---

[1]It would be more honest to say they *transform* the hierarchy problem, since one now has to explain why the extra dimensions are $10^{16} - 10^5$ times larger than the (new) fundamental scale. Possible explanations for *this* hierarchy can be found in [4].

the four-dimensional membrane is less than a TeV^{-1}. This has led to many explicit calculations quantifying the constraints that experimental data places on the magnitudes of the large extra dimensions.

In chapter 3, we calculate the rates-of-production of extra-dimensional gravitons from gluon-gluon, quark-antiquark, and electron-positron reactions in a generic, model independent fashion. We then show how these annihilation channels would affect measurements done in present and near-future lepton and hadron collider experiments, and use the results to constrain the extra-dimensional compactification scale. For the case of two extra dimensions, results from LEP2 constrain the scale to be smaller than 0.47 millimeters, while results from a next-generation linear collider could push that constraint to .012 millimeters. This work was originally presented in [2], and chapter 3 is based closely on that paper.

Arkani-Hamed and Schmaltz gave a novel solution to another familiar problem through the trapping of standard model fields in a membrane floating in a higher dimensional space. They addressed the hierarchy of Yukawa couplings, and proposed that they could be explained as a result of the slight displacement of the standard model field wavefunctions inside a four-dimensional domain wall in a higher-dimensional space. The effective four-dimensional Yukawa coupling is a product of the fundamental higher-dimensional Yukawa coupling and the overlap of the field wavefunctions. If the wavefunctions are highly peaked, a small relative shift between wavefunctions leads to a large suppression of the effective Yukawa through the smallness of the overlap of the wavefunctions. Even with a universal $O(1)$ higher-dimensional Yukawa coupling, one could produce Yukawa hierarchies through the relative displacements of the wavefunction peaks.

Although much of the recent work on fields confined to membranes derives from nonperturbative methods in string/M theory, one can actually trap chiral fermions on a domain wall using purely field-theoretic methods, and in this framework one finds that wavefunction displacements can occur in a natural way: a random collection of fermion masses in the higher-dimensional theory, which one would expect in the absence of any symmetries, leads to a random collection of displacements of the

trapped fermion wavefunctions.

In chapter 4, we explore such a model and make it concrete by finding a configuration of relative displacements which leads to the observed masses and mixings of the standard model. We find that the constraints on such a configuration lead to a prediction for the strange quark mass $m_s^{\overline{MS}}(2\ GeV) \approx (1.19) \times (V_{ub}V_{cb}/V_{us})^{1/2} \times m_b^{\overline{MS}}(m_b) \approx 120\ MeV$. This work was originally presented in [3].

1.3 Fantasy?

While the possibility that our world contains more than three spatial dimensions may seem to be unlikely at best (and ridiculous at worst), it is worth remembering that forty-four years ago the notion of an inherent handedness to the universe seemed absurd. While right-left parity appeared to be an obvious symmetry of the universe, Lee and Yang proposed that parity violation in the weak force could explain certain puzzling experimental results. Upon closer examination it was found that a parity-violating weak force was not in conflict with the approximate parity symmetry observed in nature, and less than a year after Lee and Yang proposed experiments to test their ideas, Wu demonstrated unambiguously that parity is, in fact, not a symmetry of the world. Now, parity-violating chiral gauge theories form the foundation of the standard model of particle physics. The work in this thesis reflects the real possibility that, despite the apparently three-dimensional nature of our universe, near-future measurements of supersymmetry breaking parameters, measurements of electron-positron and proton-proton cross-sections, and precision determination of the strange quark mass may indicate the presence of extra dimensions. In the context of the conventional wisdom that extra-dimensional physics (if it exists) is permanently beyond direct experimental detection, the mere possibility that the next few decades might uncover extra spatial dimensions is quite exciting!

Chapter 2

Broken Supersymmetry on a 4-d Boundary

In the strong-coupling limit of the heterotic string theory constructed by Hořava and Witten, an 11-dimensional supergravity theory is coupled to matter multiplets confined to 10-dimensional mirror planes. This structure suggests that realistic unification models are obtained, after compactification of 6 dimensions, as theories of 5-dimensional supergravity in an interval, coupling to matter fields on 4-dimensional walls. Supersymmetry breaking may be communicated from one boundary to another by the 5-dimensional fields. In this chapter, we study a toy model of this communication in which 5-dimensional super-Yang-Mills theory in the bulk couples to chiral multiplets on the walls. Using the auxiliary fields of the Yang-Mills multiplet, we find a simple algorithm for coupling the bulk and boundary fields. We demonstrate two different mechanisms for generating soft supersymmetry breaking terms in the boundary theory. We also compute the Casimir energy generated by supersymmetry breaking.

2.1 Introduction

In their recent investigation of the structure of strongly-coupled heterotic string theory, Hořava and Witten have introduced a new paradigm for models of unification

[5, 6, 7]. To construct the strong-coupling limit of the heterotic string, they began from the 11-dimensional strong-coupling limit of the Type IIA string theory. They compactified this model on S^1/Z_2, that is, on an interval of length ℓ bounded by mirror (orbifold) planes. They then argued that a 10-dimensional E_8 super-Yang-Mills theory appears on each plane. The final structure is a set of two E_8 gauge theories on the mirror planes, coupling to supergravity in the interior of the interval.

This arrangement had an immediate phenomenological advantage over the weakly coupled $E_8 \times E_8$ heterotic string theory [7]. When ℓ was increased, the low-energy value of Newton's constant decreased proportional to $1/\ell$, while the E_8 gauge coupling remained fixed. Thus, by adjustment of ℓ, one could arrange a unification of gauge and gravitational couplings. Choosing a large value of ℓ relative to the 11-dimensional Planck scale justified the use of only field-theoretic, and not intrinsically string-theoretic, degrees of freedom. At the same time, Hořava and Witten obtained reasonable values for the gauge and gravitational couplings for values of ℓ not so large, in the sense that both of these scales could be considered to be of the order of the grand unification scale of 2×10^{16} GeV inferred from the values of the gauge couplings at low energy.

In a realistic phenomenology, 6 of the transverse 10 dimensions should be compactified. Then one would obtain a 5-dimensional theory on an interval with mirror-plane boundaries. Plausibly, this theory could be described as a 5-dimensional supergravity field theory, perhaps with some additional bulk supermultiplets, coupling to matter supermultiplet fields on the walls. If ℓ is the largest dimension in this geometry, it is reasonable that the theory should make sense in the limit in which ℓ is taken to be nonzero while the finite size of the 6-dimensional compactification space is ignored.

Hořava and Witten introduced another very interesting idea on the nature of these compactifications. They pointed out that the matter theory could be at strong coupling on one boundary, and could break supersymmetry spontaneously there. Then the supersymmetry-breaking effects could be communicated to the other boundary by 11- or 5-dimensional fields. In this way, the theory on one boundary would become the 'hidden sector' for the phenomenological supersymmetry theory on the other boundary.

Hořava tried to make this mechanism of communication explicit by exhibiting a term in the 11-dimensional Lagrangian which coupled the gaugino condensate on the boundary to the 3-form gauge field C_{ABC} of the bulk supergravity theory [8]. He found that this term had a perfect-square structure

$$\Delta L = -\frac{1}{12\kappa^2} \int d^{11}x \left(\partial_{11} C_{ABC} - \frac{\sqrt{2}}{16\pi} \left(\frac{\kappa}{4\pi} \right)^{2/3} \bar{\chi} \Gamma_{ABC} \chi \, \delta(x^{11}) \right)^2 , \qquad (2.1)$$

where χ is the 10-dimensional gaugino and $8\pi\kappa^2$ is the 11-dimensional Newton constant. Hořava argued that, if the gaugino bilinear obtains a nonzero value, there is no solution for C_{ABC} which is consistent with supersymmetry.

Hořava's observations raise two interesting questions of principle. The first concerns the structure of (2.1). We might want to know how the delta function on the boundary shown in (2.1) arises. The square of this term integrated over x^{11} gives a factor $\delta(0)$ in the boundary Lagrangian. It is a puzzling issue whether this term is reasonably included in a purely field-theoretic description of the Hořava-Witten compactification, or whether the presence of this term implies that any such field-theoretic description is incomplete.

The second question comes from the fact that the communication between the two boundaries comes from the 3-form gauge field, a rather exotic agent. From the general form of the potential energy in supergravity, the 4-dimensional theory which we would obtain by compactifying 6 dimensions and then taking the limit $\ell \to 0$ must contain a direct coupling of the superpotentials on the two boundaries. We would like to know how this coupling arises, and how much of this coupling is present in the compactified theory before we take the limit $\ell \to 0$. In the standard approach to supersymmetry breaking mediated by supergravity, this coupling is the source of the soft supersymmetry-breaking mass terms for squarks and sleptons. It would be wonderful if the presence of an extended fifth dimension had specific consequences for the superparticle mass spectrum which could be verified experimentally.

We have tried to find the answers to these questions by studying a toy model in which supergravity is replaced by a Yang-Mills supermultiplet. Consider, then, 5-dimensional super-Yang-Mills theory on an interval of length ℓ bounded by mirror

planes, coupled to chiral multiplets ϕ, ϕ' on the 4-dimensional boundaries. In the limit $\ell \to 0$, this theory must have a potential energy with the D-term contribution

$$V = \frac{g^2}{2}(Q\phi^\dagger\phi + Q'\phi'^\dagger\phi')^2 \,, \tag{2.2}$$

where g is the effective 4-dimensional coupling constant and Q, Q' are the gauge charges of ϕ, ϕ'. So we can ask in this system also how much of the coupling between boundaries which is required in the limit $\ell \to 0$ survives when ℓ is kept nonzero. The related problem of coupling 5-dimensional hypermultiplets to a superpotential on the boundary has been studied previously by Sharpe [9], but, we feel, without giving the insight that we are seeking.

A convenient strategy for coupling 5-dimensional supersymmetric multiplets to a 4-dimensional boundary is to work with the off-shell supermultiplets, including auxiliary fields. Under straightforward dimensional reduction, 5-dimensional multiplets reduce to 4-dimensional $N = 2$ supermultiplets. A mirror plane, or orbifold, obtained by a Z_2 identification has lower supersymmetry, and so on such a plane a 5-dimensional multiplet should reduce to a 4-dimensional $N = 1$ supermultiplet. Nevertheless, if we have the correct off-shell multiplet, we can couple it straightforwardly to 4-dimensional fields on the boundary.

In Section 2, we will present the necessary formalism for coupling a 5-dimensional super-Yang-Mills multiplet to an orbifold boundary. We will identify the off-shell 4-dimensional supermultiplet which couples to the boundary fields and use this multiplet to construct the 4-dimensional boundary Lagrangian. In Section 3, we will discuss the role of the $\delta(0)$ terms which appear in this Lagrangian, illustrating our conclusions by some explicit one- and two-loop calculations.

In Section 4, we will use the formalism that we have developed to discuss the communication of supersymmetry breaking from one boundary to the other. We will first analyze the case in which supersymmetry is spontaneously broken by a Fayet-Iliopoulos term on one boundary. Then we will present a more involved example in which supersymmetry is communicated by loop diagrams which span the fifth dimension.

If supersymmetry is spontaneously broken, the vacuum energy can be nonzero. In general, the vacuum energy will contain a term, called the Casimir energy [10], which depends on the separation of the two boundaries. In the eventual application to supergravity, this dependence is needed to fix the size of the compact geometry. Though the case of 5-dimensional Yang-Mills theory is simpler than that of supergravity in several respects, it is still interesting to compute the Casimir energy for this case. In Section 5, we evaluate this energy for the models of the communication of supersymmetry-breaking studied in Section 4 and note the similarities of the two computations.

In Sections 3 through 5, we will be carrying out weak-coupling perturbation theory computations in the nonrenormalizable 5-dimensional Yang-Mills theory. Our attitude toward this nonrenormalizability is a pragmatic one; we will be pleased if quantities of physical interest turn out to be ultraviolet-finite at the leading order of perturbation theory. That will be true in our explicit calculations of the scalar mass term and the Casimir energy. Presumably, the higher-order corrections to these computations are cutoff-dependent and are regulated by the underlying string theory. In this discussion, we will not be concerned with effects beyond the leading nontrivial order.

Finally, in Section 6, we will discuss the relation of our formalism to Hořava's analysis and give an explanation of the coupling shown in (2.1).

Our approach to the Hořava-Witten theory complements the many attempts to understand the structure of this theory by direct analysis of the 11-dimensional Lagrangian. General properties of the strong-coupling limit of the heterotic string theory have been discussed in [11, 12, 13]. More explicit studies of the compactification of the Hořava-Witten theory have been discussed recently by several groups. Some of these analysis [14, 15, 16, 17, 18] have emphasized the connection to the venerable mechanism of supersymmetry breaking in string theory by E_8 gaugino condensation [19], while others [20, 21] have relied on the Scherk-Schwarz mechanism [22] in the bulk to provide a new source of supersymmetry breaking. Brax and Turok [23] have contributed an observation on the possibility of large hierarchies in the 5-dimensional geometry, if all of the relevant 5-dimensional fields can be made massive. We hope

that the methods of analysis that we introduce here, when generalized to supergravity, will clarify the many possible sources of supersymmetry breaking which may contribute in the Hořava-Witten approach to unification.

2.2 Bulk and boundary supermultiplets

In this section, we will set up the formalism for coupling 5-dimensional super-Yang-Mills theory to an orbifold boundary. The 5-dimensional Yang-Mills multiplet contains a vector field A^M, a real scalar field Φ, a gaugino λ^i.

In this chapter, capitalized indices M, N run over 0,1,2,3,5, lower-case indices m run over 0,1,2,3, and i, a are internal $SU(2)$ spinor and vector indices, with $i = 1, 2$, $a = 1, 2, 3$. We use a timelike metric $\eta_{MN} = \text{diag}(1,\text{-}1,\text{-}1,\text{-}1,\text{-}1)$ and take the following basis for the Dirac matrices:

$$\gamma^M = \left(\begin{pmatrix} 0 & \sigma^m \\ \bar{\sigma}^m & 0 \end{pmatrix} , \begin{pmatrix} -i & 0 \\ 0 & i \end{pmatrix} \right) , \tag{2.3}$$

where $\sigma^m = (1, \vec{\sigma})$, $\bar{\sigma}^m = (1, -\vec{\sigma})$. Though it is conventional in the literature to use raised and lowered spinor indices, we find it less confusing to write out explicitly the 2×2 and 4×4 charge conjugation matrices

$$c = -i\sigma^2 , \qquad C = \begin{pmatrix} c & 0 \\ 0 & c \end{pmatrix} . \tag{2.4}$$

In 5-dimensional supersymmetry, it is convenient to rewrite 4-component Dirac spinors as symplectic-Majorana spinors, Dirac fermions which carry an $SU(2)$ spinor index and satisfy the constraints

$$\psi^i = c^{ij} C \bar{\psi}^{jT} . \tag{2.5}$$

A symplectic-Majorana spinor can be decomposed into 4-dimensional chiral spinors according to

$$\psi^i = \begin{pmatrix} \phi^i_L \\ \phi^i_R \end{pmatrix} \tag{2.6}$$

where $\phi^i_{L,R}$ are two-component spinors connected by

$$\phi^i_L = c^{ij} c \phi^{j*}_R , \qquad \phi^i_R = c^{ij} c \phi^{j*}_L .$$ (2.7)

Symplectic-Majorana spinors ψ^i, χ^i satisfy the identity

$$\overline{\psi}^i \gamma^M \cdots \gamma^P \chi^j = -c^{ik} c^{jl} \overline{\chi}^l \gamma^P \cdots \gamma^M \psi^k ,$$ (2.8)

including the minus sign from fermion interchange.

In this notation, the 5-dimensional Yang-Mills multiplet is extended to an off-shell multiplet by adding an $SU(2)$ triplet X^a of real-valued auxiliary fields [24]. Write the members of the multiplet as matrices in the adjoint representation of the gauge group: $A^M = A^{MA} t^A$, *etc.* The supersymmetry transformation laws are

$$
\begin{aligned}
\delta_\xi A^M &= i\overline{\xi}^i \gamma^M \lambda^i \\
\delta_\xi \Phi &= i\overline{\xi}^i \lambda^i \\
\delta_\xi \lambda^i &= (\sigma^{MN} F_{MN} - \gamma^M D_M \Phi)\xi^i - i(X^a \sigma^a)^{ij} \xi^j \\
\delta_\xi X^a &= \overline{\xi}^i (\sigma^a)^{ij} \gamma^M D_M \lambda^j - i[\Phi, \overline{\xi}^i (\sigma^a)^{ij} \lambda^j] ,
\end{aligned}
$$ (2.9)

where the symplectic-Majorana spinor ξ^i is the supersymmetry parameter, $D_M \Phi \equiv \partial_M \Phi - i[A_M, \Phi]$ (and similarly for $D_M \lambda$), and $\sigma^{MN} \equiv \frac{1}{4}[\gamma^M, \gamma^N]$.

Now we would like to project this structure down to a 4-dimensional $N = 1$ supersymmetry transformation acting on fields on the orbifold wall. In a field theory description, an orbifold at $x^5 = 0$ is described by imposing the boundary condition on bulk fields $a(x, x^5)$

$$a(x^m, x^5) = P a(x^m, -x^5)$$ (2.10)

where P is an intrinsic parity equal to ± 1. The quantum number P must be assigned to fields in such a way that it leaves the bulk Lagrangian invariant. Then fields of $P = -1$ vanish on the walls but have nonvanishing derivatives $\partial_5 a$. Note that, since A^5 vanishes on the boundary, $\partial_5 = D_5$ on the boundary and $\partial_5 a$ is gauge-covariant.

Let ξ_L^1 be the supersymmetry parameter of the $N = 1$ supersymmetry transformation on the wall. Then the P assignments of the fields in the bulk supermultiplet are determined as follows:

	$P = +1$	$P = -1$
ξ	ξ_L^1	ξ_L^2
A^M	A^m	A^5
Φ	-	Φ
λ^i	λ_L^1	λ_L^2
X^a	X^3	$X^{1,2}$

$$(2.11)$$

On the wall at $x^5 = 0$, the supersymmetry transformation (2.9) reduces to the following transformation of the even-parity states generated by ξ_L^1:

$$
\begin{aligned}
\delta_\xi A^m &= i\xi_L^{1\dagger}\bar{\sigma}^m\lambda_L^1 - i\lambda_L^{1\dagger}\bar{\sigma}^m\xi_L^1 \\
\delta_\xi \lambda_L^1 &= \sigma^{mn}F_{mn}\xi_L^1 - i(X^3 - \partial_5\Phi)\xi_L^1 \\
\delta_\xi X^3 &= \xi_L^{1\dagger}\bar{\sigma}^m D_m\lambda_L^1 - i\xi_L^{1\dagger}c\partial_5\lambda_L^{2*} + h.c. \\
\delta_\xi \partial_5\Phi &= -i\xi_L^{1T}c\partial_5\lambda_L^2 - i\xi_L^{1\dagger}c\partial_5\lambda_L^{2*} \, .
\end{aligned}
$$

$$(2.12)$$

The last two equations imply

$$
\delta_\xi(X^3 - \partial_5\Phi) = \xi_L^{1\dagger}\bar{\sigma}^m D_m\lambda_L^1 + h.c. \, .
$$

$$(2.13)$$

These are just the transformation laws for an $N = 1$ 4-dimensional vector multiplet [25], with A^m, λ_L^1, and $(X^3 - \partial_5\Phi)$ transforming as the vector, gaugino, and auxiliary D fields.

The appearance of the quantity $\partial_5\Phi$ in the auxiliary field should not be a surprise. It is the expectation value of this quantity that breaks supersymmetry in the Scherk-Schwarz mechanism [22]. Thus, $\partial_5\Phi$ should appear in the order parameter of supersymmetry breaking.

Now it is obvious how to couple the 5-dimensional gauge multiplet to 4-dimensional

chiral multiplets on the boundary. We write the Lagrangian as

$$S = \int d^5x \left\{ \mathcal{L}_5 + \sum_i \delta(x^5 - x_i^5)\mathcal{L}_{4i} \right\} , \tag{2.14}$$

where the sum includes the walls at $x_i^5 = 0, \ell$. The bulk Lagrangian should be the standard one for a 5-dimensional super-Yang-Mills multiplet,

$$\begin{aligned}
\mathcal{L}_5 &= \frac{1}{g^2}\Big(-\frac{1}{2}\text{tr}(F_{MN})^2 + \text{tr}(D_M\Phi)^2 + \text{tr}(\overline{\lambda}i\gamma^M D_M\lambda) \\
&\quad + \text{tr}(X^a)^2 - \text{tr}(\overline{\lambda}[\Phi,\lambda])\Big) ,
\end{aligned} \tag{2.15}$$

with $\text{tr}[t^A t^B] = \delta^{AB}/2$. The bulk fields should be constrained to satisfy the boundary conditions (2.10) at the walls. Since the supersymmetry generated by ξ_L^1 relates fields with the same boundary conditions, this $N = 1$ supersymmetry is an invariance of (2.15) under the constraint.

The boundary Lagrangian should have the standard form of a four-dimensional chiral model built from supermultiplets (ϕ, ψ_L, F). Here and in the rest of the chapter, it is important to distinguish boundary chiral scalar fields, which we will label by ϕ, from the bulk scalar field Φ. The explicit form of this boundary Lagrangian is

$$\begin{aligned}
\mathcal{L}_4 &= D_m\phi^\dagger D^m\phi + \psi_L^\dagger i\overline{\sigma}^m D_m\psi_L + F^\dagger F \\
&\quad - \sqrt{2}i\left(\phi^\dagger \lambda_L^T c\psi_L + \psi^\dagger c\lambda_L^*\phi\right) + \phi^\dagger D\phi ,
\end{aligned} \tag{2.16}$$

with $D_m = (\partial_m - iA_m)$, and with with the gauge fields (A_m, λ_L, D) replaced by the boundary values of the bulk fields $(A_m, \lambda_L^1, X^3 - \partial_5\Phi)$. The boundary Lagrangian $\mathcal{L}_4$ is invariant by itself under an $N = 1$ supersymmetry transformation of the boundary fields and the supersymmetry transformation (2.12) of the bulk fields. Thus, the complete action (2.14) is $N = 1$ supersymmetric.

In principle, we could add to (2.14) additional terms involving a four-dimensional integral of the boundary values of the vector fields, or terms coupling the chiral fields to higher ∂_5 derivatives of the vector fields at the boundary. These terms would correspond to contributions that are more singular at the boundary that the ones we

have considered. For our present purposes, we only point out that these terms are not necessary for supersymmetry, and we neglect them from here on. We will show in explicit calculations that the terms we have written suffice to give amplitudes which converge to the correct 4-dimensional limits as $\ell \to 0$. With the action (2.14), the boundary scalar field ϕ at $x^5 = 0$ couples to the auxiliary field X^3 through the terms

$$\int d^5x \left\{ \frac{1}{g^2} \text{tr}(X^3)^2 + \delta(x^5)\phi^\dagger(X^3 - \partial_5\Phi)\phi \right\} . \tag{2.17}$$

The field Φ is a dynamical field in the interior, but X^3 is an auxiliary field and may be integrated out. This gives a boundary Lagrangian of the form

$$\int d^4x \left\{ -\phi^\dagger(\partial_5\Phi)\phi - \frac{1}{2}(\phi^\dagger t^A \phi)^2 \delta(0) \right\} . \tag{2.18}$$

Thus, our formalism does contain singular terms proportional to $\delta(0)$ on the boundary, which arise naturally from integrating out the auxiliary fields. In principle, the complete description of the orbifold wall in string theory could contain additional couplings involving higher derivatives ∂_5 of the bulk fields and representing a finite thickness and a shape of the wall. However, the Lagrangian we have written, with the $\delta(0)$ but no additional singular terms, is a completely self-consistent supersymmetric system.

2.3   Bulk and boundary perturbation theory

In the previous section, we have found that singular terms proportional to $\delta(0)$ on the boundary arise naturally when bulk and boundary fields are coupled supersymmetrically. What is still unclear is whether these terms can lead to sensible results when one performs computations in this theory, or whether these terms signal the breakdown of a purely field-theoretic description. We believe that these singular terms do make sense at the field theory level. Their role is to provide counterterms which are necessary in explicit calculations to maintain supersymmetry. In this section, we will illustrate this conclusion with some explicit calculations in perturbation theory.
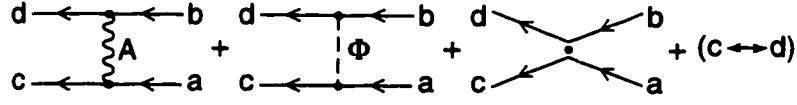
Figure 2.1: Feynman diagrams contributing to the scattering process $\phi\phi \to \phi\phi$.

As a first, simplest, example, consider the scattering amplitude for scalars on a wall. The Feynman diagrams contributing to the process $\phi_a + \phi_b \to \phi_c + \phi_d$ are shown in Figure 2.1. The propagator of a free massless bulk field is

$$\left\langle a(x, x^5) a(y, y^5) \right\rangle = \int_{k5} \frac{i}{k^2 - (k^5)^2} e^{-ik\cdot(x-y)} \left(e^{ik^5(x^5-y^5)} + P e^{ik^5(x^5+y^5)} \right) , \qquad (2.19)$$

where

$$\int_{k5} = \int \frac{d^4k}{(2\pi)^4} \frac{1}{2\ell} \sum_{k^5} , \qquad (2.20)$$

with k^5 summed over the values $\pi m/\ell$, $m =$ integer. Here and in the rest of our discussion, k represents the 4-dimensional momentum components of k^M.

The sum of diagrams in Figure 2.1 is given by

$$
\begin{aligned}
i\mathcal{M}(\phi_a + \phi_b \to \phi_c + \phi_d) &= -ig^2 t^A_{ca} t^A_{db} \left(\frac{1}{2\ell} \sum_{k^5} \frac{(k^5)^2}{(p_c - p_a)^2 - (k^5)^2} + \delta(0) \right. \\
&\quad \left. - \frac{1}{2\ell} \sum_{k^5} \frac{(p_c + p_a) \cdot (p_d + p_b)}{(p_c - p_a)^2 - (k^5)^2} \right) + (c \leftrightarrow d) . \quad (2.21)
\end{aligned}
$$

If we represent

$$\delta(0) = \frac{1}{2\ell} \sum_{k^5} 1 = \frac{1}{2\ell} \sum_{k^5} \frac{k^2 - (k^5)^2}{k^2 - (k^5)^2} , \qquad (2.22)$$

the first two terms have a neat cancellation and we find the finite result

$$
\begin{aligned}
i\mathcal{M}(\phi_a + \phi_b \to \phi_c + \phi_d) &= -ig^2 t^A_{ca} t^A_{db} \left(\frac{1}{2\ell} \sum_{k^5} \frac{(p_c - p_a)^2 - (p_c + p_a) \cdot (p_d + p_b)}{(p_c - p_a)^2 - (k^5)^2} \right) \\
&\quad + (c \leftrightarrow d)
\end{aligned}
$$
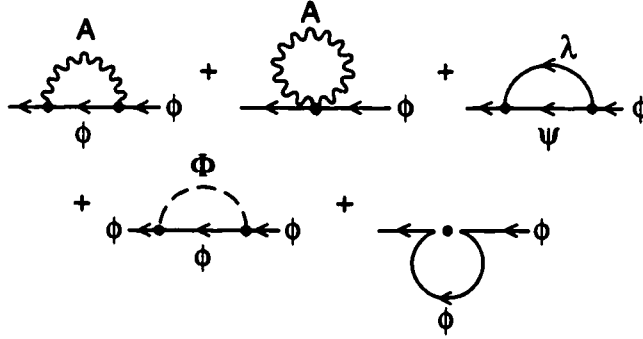
Figure 2.2: Feynman diagrams contributing to the ϕ self-energy at one-loop order.

$$= -ig^2 t^A_{ca} t^A_{db} \left(\frac{1}{2\ell} \sum_{k^5} \frac{-2u}{t - (k^5)^2} \right) + (c \leftrightarrow d) .$$ (2.23)

If $\ell \to 0$ with the dimensionless coupling g^2/ℓ fixed, the terms with $k^5 \neq 0$ become negligible. Then we recover the scalar particle scattering amplitude of a 4-dimensional $N = 1$ supersymmetric gauge theory.

As a second example, consider the self-energy of the scalar ϕ, computed at the one-loop level. By supersymmetry, the ϕ cannot obtain a mass in perturbation theory, but it is interesting to see explicitly how the cancellation occurs. The Feynman diagrams for the ϕ self-energy are shown in Figure 2.2. The first four diagrams all involve one field that propagates in four dimensions and one field that propagates in the fifth dimension. Thus, if p is the external 4-momentum, all of these diagrams will have the structure

$$-iM^2(p^2) = g^2 t^A t^A \int_{k5} \frac{1}{k^2 - (k^5)^2} \frac{1}{(p - k)^2} N(k, k^5, p) ,$$ (2.24)

where N is a polynomial in momenta. Using the representation (2.22), we can bring the last diagram into this form as well. Then the five diagrams give contributions

$$N = -(2p - k)^2 + 4(p - k)^2 - 4k \cdot (k - p) + (k^5)^2 + (k^2 - (k^5)^2)$$

$$= 0 .$$ (2.25)
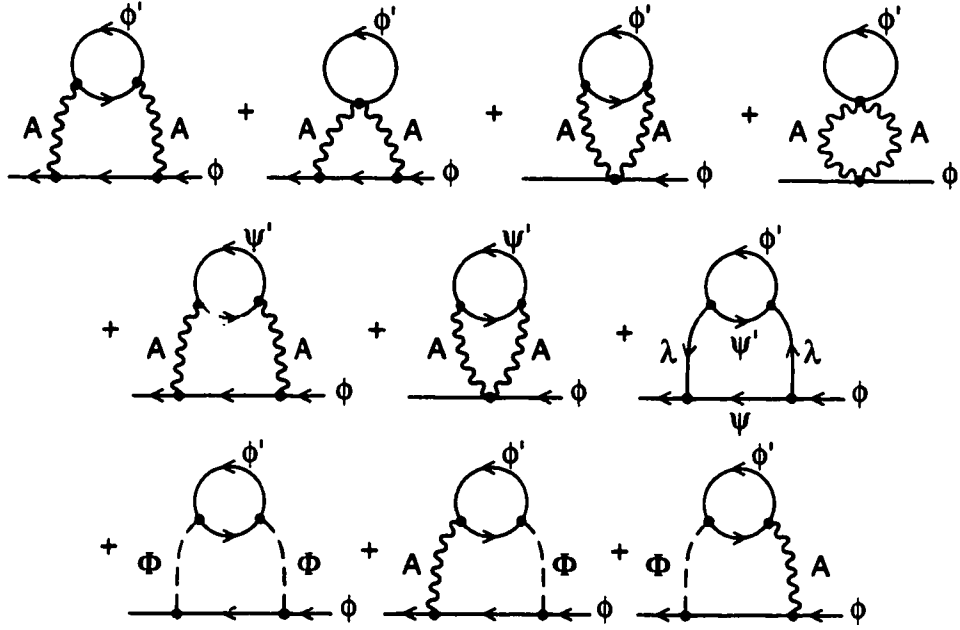
Figure 2.3: Feynman diagrams contributing to the mass shift of a scalar ϕ on one wall due to loop effects of the supermultiplet on the other wall.

Here the $\delta(0)$ term enters quite explicitly as a counterterm which cancels the singular behavior of the Φ exchange diagram and thus allows the complete cancellation required by supersymmetry.

To prepare for the next section, it will be useful to illustrate one more cancellation required by supersymmetry. Consider the renormalization of the mass of a scalar ϕ on one wall due to loop diagrams involving the supermultiplet on the other wall. This mass shift is given by the sum of the two-loop diagrams shown in Figure 2.3. In our discussion of these diagrams, we will assign the chiral fields ϕ at $x^5 = 0$ to the representation R of the gauge group, and we will assign the fields ϕ' at $x^5 = \ell$ to the representation R'.

The diagrams of Figure 2.3 form a gauge-invariant set. We might characterize them as the diagrams of order $g^4 N$, where N is the number of matter multiplets on the second wall. Thus, by supersymmetry, their sum must vanish.

It is not difficult to see this explicitly. Since we are interested in the shift of the

ϕ mass term, we can set the external momentum equal to zero. Then let q be the loop momentum of the matter loop on the wall at $x^5 = \ell$, Let (k, k^5) and $(k, \hat{k}^5)$ be the momenta carried by the two propagators of the gauge multiplet that connect the two walls. These momenta are quantized, with

$$k^5 = \pi n/\ell , \qquad \hat{k}^5 = \pi \hat{n}/\ell , \tag{2.26}$$

but the integers n and $\hat{n}$ are summed over independently, since k^5 is not conserved in the interaction of bulk fields with the walls. Then all of the diagrams shown in Figure 2.3 can be written in the form

$$-iM^2 = ig^4 C_2(R)C(R') \int_q \int_{k55} \frac{N(k, k^5, \hat{k}^5, q)}{(k^2)(k^2 - (k^5)^2)(k^2 - (\hat{k}^5)^2)(q^2)((q-k)^2)} , \tag{2.27}$$

where N is a polynomial in momenta, $C(R')\delta^{AB} = \mathrm{tr}_{R'}[t^A t^B]$ is the sum over the gauge quantum numbers of the multiplet at $x^5 = \ell$, the integral over q is a simple 4-dimensional momentum integral, and

$$\int_{k55} = \int \frac{d^4k}{(2\pi)^4} \frac{1}{2\ell} \sum_n \frac{1}{2\ell} \sum_{\hat{n}} 4 \cdot (-1)^{n+\hat{n}} . \tag{2.28}$$

This expression includes the k^5-dependence of the propagators, obtained by evaluating (2.19) at $x^5 = 0$, $y^5 = \ell$.

To see that the diagrams of this set must cancel, it is easiest to compare this calculation to the corresponding two-loop mass renormalization in four dimensions. The diagrams on the first two lines of Figure 2.3 contain, from the five-dimensional gauge multiplet, only the propagators of the fields A_m and λ_L^1 which appear in a 4-dimensional gauge multiplet. Thus, their contributions to the numerator polynomial N are exactly those of the corresponding diagrams in 4 dimensions. To treat the last three diagrams, we note the identity

$$0 = \frac{1}{2\ell} \sum_{k^5} (-1)^n = \frac{1}{2\ell} \sum_{k^5} (-1)^n \frac{k^2 - (k^5)^2}{k^2 - (k^5)^2} , \tag{2.29}$$

since the second term is a representation of $\delta(x^5)$ evaluated at $x^5 = \ell$. Each Φ propagator comes with a factor $(k^5)^2$, due to the couplings (2.18) at each wall. The identity (2.29) allows us to replace this $(k^5)^2$ by k^2. Then each diagram gives the same contribution to the numerator as the corresponding 4-dimensional diagram with the Φ replaced by a D-term interaction. Thus, the numerator polynomial N turns out to be exactly the one that appears in the 4-dimensional calculation.

At this point, we know that the integral (2.27) must vanish. It is not difficult to evaluate the various contributions to the numerator and to see that they cancel. In the Appendix, we give a formula for the numerator factor N from which this can be verified explicitly.

2.4   Wall to Wall Supersymmetry Breaking

We have now described and tested an explicit form for the coupling of 4-dimensional supermultiplets on the boundary to gauge supermultiplets in the bulk. Now we can use this formalism to see how supersymmetry breaking on one wall is communicated to the other wall to provide soft supersymmetry-breaking terms. In this section, we will give two examples of such communication, one through a direct tree-level coupling and the other induced by loop effects.

The simplest example of the communication of supersymmetry breaking is obtained in a theory in which the wall at $x^5 = \ell$ contains no boundary matter fields. We choose the gauge group to be $U(1)$ and write a Fayet-Iliopoulos D term on this boundary. With the identification of the D term given in Section 2, the following boundary action preserves $N = 1$ supersymmetry:

$$\mathcal{L}_4 = \kappa(X^3 - \partial_5\Phi) . \tag{2.30}$$

Integrating out the auxiliary field X^3 leads to a $\delta(0)$ term which is an irrelevant constant. The dynamical Φ field is affected by (2.30) in a manner that we can compute from the action

$$S = \int d^5x \left\{ \frac{1}{2g^2}(\partial_M\Phi)^2 - \kappa\partial_5\Phi\delta(x^5 - \ell) \right\} . \tag{2.31}$$

Varying this action with respect to Φ, we find that the Fayet-Iliopoulos term induces a background expectation value of Φ which depends only on x^5 and satisfies the equation

$$\frac{1}{g^2}\partial_5^2 \langle \Phi \rangle + \kappa \partial_5 \delta(x^5 - \ell) = 0 . \tag{2.32}$$

In solving this equation, we should remember that the geometry with mirror planes arose from a identification of points in a compactification of x^5 on a circle. Thus, $\langle \Phi(x^5) \rangle$ must be a periodic function of x^5 with period 2ℓ and so $\partial_5\Phi$ must integrate to zero around the circle. This boundary condition requires that we choose as the solution to (2.32)

$$\partial_5 \langle \Phi \rangle = -g^2 \kappa \left(\delta(x^5 - \ell) - \frac{1}{2\ell} \right) . \tag{2.33}$$

Inserting this result into the D-term coupling on the wall at $x^5 = 0$, given by (2.17), we find a scalar mass term given by

$$M_\phi^2 = g^2 Q \frac{\kappa}{2\ell} , \tag{2.34}$$

where Q is the $U(1)$ charge of the scalar field, with no corresponding mass term induced for the fermions on the wall. If the dynamics on the wall at $x^5 = \ell$ gives a D-term of fixed magnitude there, the Φ field transfers this across the fifth dimension to create a soft scalar mass term on the wall at $x^5 = 0$.

One subtlety of the Fayet-Iliopoulos mechanism of supersymmetry breaking is that the symmetry breaking D term can sometimes be compensated by shifting the vacuum expectations value of a scalar field. We can see a similar possibility here. Generalize the previous model to include several chiral multiplets ϕ_i on the wall at $x^5 = 0$, and additional chiral multiplets ϕ_j on the wall at $x^5 = \ell$. (As always, it is important to distinguish between the boundary scalar fields ϕ and the bulk field Φ.) Assign these multiplets the charges Q_i, Q_j under the $U(1)$ symmetry. In the most general situation, all of the scalar fields might acquire vacuum expectation values. Then the Lagrangian for Φ will take the form

$$S = \int d^5x \Big\{ \frac{1}{2g^2}\left((X^3)^2 + (\partial_M\Phi)^2 \right) + (\sum_i Q_i\phi_i^\dagger\phi_i)(X^3 - \partial_5\Phi)\delta(x^5)$$

$$+(\kappa + \sum_j Q_j \phi_j^\dagger \phi_j)(X^3 - \partial_5 \Phi)\delta(x^5 - \ell)\bigg\} \; . \tag{2.35}$$

For simplicity, we assume that the ϕ_i and ϕ_j are represented only by vacuum expectation values that are independent of position on the walls. Then varying the action (2.35) with respect to Φ gives an equation analogous to (2.32) whose solution is

$$\partial_5 \langle \Phi \rangle \;=\; -g^2 \bigg[(\sum_i Q_i \phi_i^\dagger \phi_i) \left(\delta(x^5) - \frac{1}{2\ell} \right) $$

$$+ (\kappa + \sum_j Q_j \phi_j^\dagger \phi_j) \left(\delta(x^5 - \ell) - \frac{1}{2\ell} \right) \bigg] \; . \tag{2.36}$$

This result reduces to (2.33) when we turn off the expectation values of the ϕ_i and ϕ_j. If we insert this expression into (2.35), and also integrate out the auxiliary field X^3, the various $\delta(0)$ terms cancel, leaving behind

$$S = \int d^5 x \bigg\{ -\frac{g^2}{4\ell}(\kappa + \sum_i Q_i \phi_i^\dagger \phi_i + \sum_j Q_j \phi_j^\dagger \phi_j)^2 \bigg\} \; . \tag{2.37}$$

To minimize the vacuum energy, we must set the various vacuum expectation values to the supersymmetric condition

$$\kappa + \sum_i Q_i \phi_i^\dagger \phi_i + \sum_j Q_j \phi_j^\dagger \phi_j = 0 \; , \tag{2.38}$$

if this is possible.

If the supersymmetric theory on the wall at $x^5 = \ell$ breaks supersymmetry spontaneously without inducing a D term, it is necessary to go to a higher order in perturbation theory to find the supersymmetry-breaking communication. If supersymmetry breaking causes a mass splitting among chiral supermultiplets on the wall at $x^5 = \ell$, and these multiplets couple to the gauge field in the bulk, then the diagrams shown in Figure 2.3 induce a supersymmetry-breaking mass for scalars on the wall at $x^5 = 0$. Since, in the scheme we are studying, the particle number of a chiral multiplet at $x^5 = 0$ is conserved, this is the only soft supersymmetry-breaking term that can be generated.

The generation of the scalar mass term in this example is very similar to that in 'gauge-mediated' 4-dimensional models of supersymmetry breaking [26]. The same set of diagrams appears, with only the difference that our gauge fields live in 5 dimensions.

To illustrate the computation of these diagrams, we study the simplest multiplet which appears in models of gauge-mediation. We introduce on the wall at $x^5 = \ell$ two chiral superfields $(\phi', \overline{\phi}')$ which transform under the gauge group as a vectorlike representation $(R' + \overline{R}')$. (Recall that we are using R to denote representations of the chiral fields ϕ at $\ell = 0$.) We give this multiplet a supersymmetric mass m and induce an additional mass term for the scalar fields from the vacuum expectation value of an F-term. Then the fermions have a Dirac mass m, while the bosons have a (mass)^2 matrix

$$M^2 \begin{pmatrix} \phi' \\ \overline{\phi}^{*\prime} \end{pmatrix} = \begin{pmatrix} m^2 & m^2 x \\ m^2 x & m^2 \end{pmatrix} \begin{pmatrix} \phi' \\ \overline{\phi}^{*\prime} \end{pmatrix} . \tag{2.39}$$

The eigenvectors of this matrix are species ϕ'_+, ϕ'_- in the representation R'. Thus, we find the mass spectrum on the wall at $x^5 = \ell$,

$$m^2(\phi'_+) = m^2_+ , \qquad m^2(\phi'_-) = m^2_- , \qquad m^2(\psi') = m^2 , \tag{2.40}$$

with $m^2_\pm = m^2(1 \pm x)$. This spectrum satisfies $\mathrm{str}[M^2] = 0$. Our calculation will follow closely the discussion of gauge-mediated scalar masses in this model given by Martin [27]. It is straightforward to generalize our calculation to models of supersymmetry breaking with nonvanishing supertrace. However, in that case, the scalar masses induced by gauge-mediation are cutoff-dependent even in 4 dimensions [28]. Similar divergences appear also in the 5-dimensional case.

To compute the scalar mass, we repeat the calculation of the diagrams in Figure 2.3, now assigning to the particles in the loop the mass spectrum described in the previous paragraph. As in the previous section, the identity (2.29) can be used to replace $(k^5)^2$ by k^2 in the numerator of the diagrams with Φ exchange. Then the result reduces to a sum of two-loop scalar integrals, just as in the 4-dimensional case.
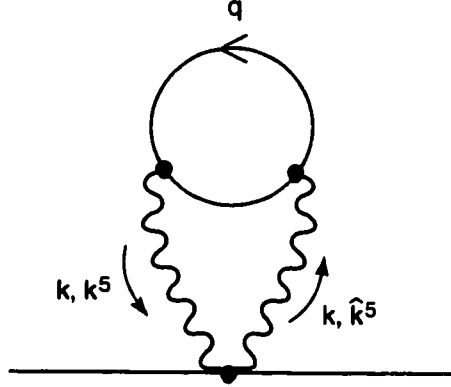
Figure 2.4: The basic integral which appears in the two-loop contribution to the scalar field mass.

To write the result precisely, define [29]

$$(m_1 m_2 | m_3 | m_4) = \int \frac{d^d k}{(2\pi)^d} \int \frac{d^d q}{(2\pi)^d} \frac{1}{k^2 + m_1^2} \frac{1}{k^2 + m_2^2} \frac{1}{q^2 + m_3^2} \frac{1}{(q-k)^2 + m_4^2} \quad (2.41)$$

to be the Euclidean (Wick-rotated) scalar two-loop integral with four propagators, and denote Euclidean scalar integrals with additional or fewer propagators by brackets with more or fewer labels m_i. In our calculation, k^5 is summed over the values $\pi n/\ell$; denote the sum in (2.28) as

$$[\mathcal{A}] = \frac{1}{2\ell} \sum_n \frac{1}{2\ell} \sum_{\hat{n}} 4 \cdot (-1)^{n+\hat{n}} \mathcal{A}(k^5, \hat{k}^5) . \quad (2.42)$$

The basic scalar integral shown in Figure 2.4 is then written

$$[(k^5 \hat{k}^5 | m_1 | m_2)] . \quad (2.43)$$

Finally, though a term with k^2 in the numerator can be reduced to scalar integrals, it is more convenient to retain this factor under the integral in (2.41). By abuse of notation, we will write a term with k^2 in the numerator as, for example, $[k^2 (k^5 \hat{k}^5 | m_2 | m_3)]$.

Using the notation, the scalar mass due to the diagrams of Figure 2.3 is

$$m_\phi^2 = -g^4 C_2(R)C(R')[k^2\mathcal{R} + 4\mathcal{S}] ,$$ (2.44)

where

$$
\begin{aligned}
\mathcal{R} &= (k^5\hat{k}^5|m_+|m_+) + (k^5\hat{k}^5|m_-|m_-) \\
&\quad +2(k^5\hat{k}^5|m_+|m_-) + 4(k^5\hat{k}^5|m|m) \\
&\quad -4(k^5\hat{k}^5|m_+|m) - 4(k^5\hat{k}^5|m_-|m) \\
\mathcal{S} &= m_+^2 \left\{ (k^5\hat{k}^5|m_+|m_+) - (k^5\hat{k}^5|m_+|m) \right\} \\
&\quad -m^2 \left\{ (k^5\hat{k}^5|m|m) - (k^5\hat{k}^5|m_+|m) \right\} \\
&\quad +m_-^2 \left\{ (k^5\hat{k}^5|m_-|m_-) - (k^5\hat{k}^5|m_-|m) \right\} \\
&\quad -m^2 \left\{ (k^5\hat{k}^5|m|m) - (k^5\hat{k}^5|m_-|m) \right\} .
\end{aligned}
$$ (2.45)

This expression is full of cancellations which reflect the fact that the answer vanishes when the mass spectrum is supersymmetric. To evaluate this answer more explicitly, we must perform the sums over k^5 and $\hat{k}^5$ and then carry out the two four-dimensional integrals.

The sums can be performed conveniently using a standard trick from finite temperature field theory. Write a contour integral representation

$$\frac{1}{2\ell} \sum_n 2(-1)^n \frac{1}{k^2 + (k^5)^2} = \oint \frac{dk^5}{2\pi} \frac{2e^{ik^5\ell}}{e^{2ik^5\ell} - 1} \frac{1}{k^2 + (k^5)^2} ,$$ (2.46)

where the contour encloses the poles of the integrand at $k^5 = \pi n/\ell$. Draw the contour as a line from left to right just below the real axis and another line from right to left just above this axis. Push the first line down and pick up the pole at $k^5 = -ik$; push the second line up and pick up the pole at $k^5 = ik$. We find two identical contributions which sum to

$$\frac{1}{k} \frac{1}{\sinh k\ell} .$$ (2.47)

This manipulation can be performed separately on each of the propagators joining

the two walls.

At the same time, the scalar integrals over the momentum q can be evaluated explicitly. Define the function $b(k^2, m_1^2, m_2^2)$ by

$$\int \frac{d^d q}{(2\pi)^d} \frac{1}{q^2 + m_1^2} \frac{1}{(q-k)^2 + m_2^2} = \frac{1}{(4\pi)^{d/2}} \{ \frac{2}{\epsilon} - \gamma - b(k^2, m_1^2, m_2^2) + \mathcal{O}(\epsilon) \} \quad (2.48)$$

for $d = 4 - \epsilon$. When we evaluate the loop integrals on the wall in (2.45), the divergent terms cancel and we are left with differences of these scalar functions,

$$
\begin{aligned}
\mathcal{R} \rightarrow R(k^2) &= b(k^2, m_+^2, m_+^2) + b(k^2, m_-^2, m_-^2) \\
&\quad + 2b(k^2, m_+^2, m_-^2) + 4b(k^2, m^2, m^2) \\
&\quad - 4b(k^2, m_+^2, m^2) - 4b(k^2, m_-^2, m^2) \\
\mathcal{S} \rightarrow S(k^2) &= m_+^2 \{ b(k^2, m_+^2, m_+^2) - b(k^2, m_+^2, m^2) \} \\
&\quad - m^2 \{ b(k^2, m^2, m^2) - b(k^2, m_+^2, m^2) \} \\
&\quad + m_-^2 \{ b(k^2, m_-^2, m_-^2) - b(k^2, m_-^2, m^2) \} \\
&\quad - m^2 \{ b(k^2, m^2, m^2) - b(k^2, m_-^2, m^2) \} \ .
\end{aligned} \quad (2.49)
$$

If we then define

$$P(k^2) = k^2 R(k^2) + 4S(k^2) \ , \quad (2.50)$$

then the combination of these two tricks brings (2.44) into the form of an integral over k. Since this integral is spherically symmetric, we can replace $d^4 k = 2\pi^2 dk k^3$ and write (2.44) as

$$m_\phi^2 = 2 \left(\frac{g^2}{(4\pi)^2} \right)^2 C_2(R) C(R') \int_0^\infty dk k \frac{1}{\sinh^2 k\ell} P(k^2) \ . \quad (2.51)$$

The function $P(k^2)$ is elementary, and it is not difficult to work out its asymptotic behavior for large and for small k^2. We present these formulae in the Appendix. It is relevant that $P(k^2) \sim k^2$ as $k^2 \rightarrow 0$, so that $P(k^2)$ is a field-strength renormalization [30] (as the notation is meant to suggest). As $k^2 \rightarrow \infty$, $P(k^2) \sim \log(k^2/m^2)/k^2$. With this information, one can work out the asymptotic behaviors of m_ϕ^2.

For small ℓ, we might expect to go back the the 4-dimensional situation. Formally, taking $\ell \to 0$ in (2.47) turns this expression into

$$\frac{2}{2\ell}\frac{1}{k^2} \, , \tag{2.52}$$

which is the $k^5 = 0$ term in the sum (2.46). Using the explicit asymptotic behavior of $P(k^2)$, we can see that the integral (2.51) remains well-defined in this limit. Thus, the manipulation is permitted and the result for m_ϕ^2 becomes just the 4-dimensional gauge-mediation result with the replacement

$$\left(\frac{g^2}{(4\pi)^2}\right)^2 \to \left(\frac{g^2}{(4\pi)^2}\right)^2 \frac{1}{\ell^2} \, . \tag{2.53}$$

We will write out this result explicitly below. Note that g^2/ℓ is the effective 4-dimensional gauge coupling obtained by simple dimensional reduction.

Another way to derive this result is to show that, for $\ell \to 0$, all terms in the sum over k^5 and $\hat{k}^5$ are explicitly suppressed by the factor ℓ^2 except for the term with $k^5 = \hat{k}^5 = 0$. Again, the asymptotic behavior $P(k^2) \sim 1/k^2$ is necessary to complete this argument.

For large ℓ, the hyperbolic sine in the denomination of (2.51) cuts off the integrand for all but very small k. Thus, we can find the asymptotic behavior by replacing $P(k^2)$ by its leading term for small k^2, which is proportional to k^2. This gives a result proportional to

$$\left(\frac{g^2}{(4\pi)^2}\right)^2 \frac{1}{\ell^4} \, . \tag{2.54}$$

Working out all of the details (with the help of some formulae from the Appendix), we find, as $m\ell \to 0$, the 4-dimensional form [27, 31]

$$
\begin{aligned}
m_\phi^2 &= 2C_2(R)C(R') \left(\frac{g^2}{(4\pi)^2}\right)^2 \cdot \frac{m^2}{\ell^2} \\
&\quad \cdot \left\{ 2(1+x)\left[\log(1+x) - 2\text{Li}_2(\frac{x}{1+x}) + \frac{1}{2}\text{Li}_2(\frac{2x}{1+x})\right] \right.
\end{aligned}
$$
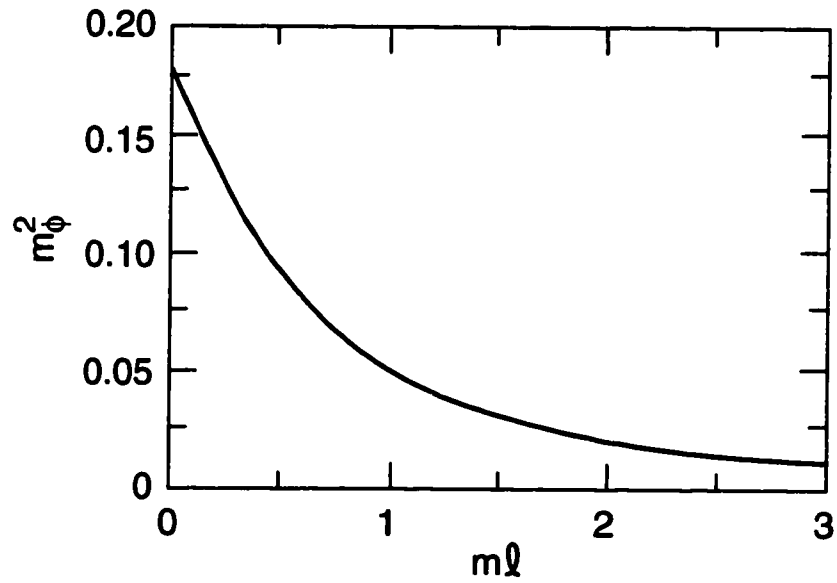
m_ϕ^2 is plotted in units of $2C_2(R)C(R')(g^2/(4\pi)^2)^2) \cdot (m^2/\ell^2))$

Figure 2.5: Behavior of the induced supersymmetry breaking mass for scalars at $x^5 = 0$ as a function of ℓ.

$$+(x \leftrightarrow -x) \Bigg\} \ , \tag{2.55}$$

where $\mathrm{Li}_2(x)$ is the dilogarithm, and, as $m\ell \to \infty$,

$$m_\phi^2 = 2C_2(R)C(R') \left(\frac{g^2}{(4\pi)^2}\right)^2 \cdot \frac{1}{\ell^4} \cdot \zeta(3)$$

$$\cdot \left\{ \frac{3}{2} \left[\frac{4 + x - 2x^2}{x^2} \log(1 + x) - \frac{4 - x}{x} \right] + (x \leftrightarrow -x) \right\} \ . \tag{2.56}$$

In both of these expressions, the quantity in brackets tends to x^2 as $x \to 0$. We see that the induced soft supersymmetry breaking mass term crosses over from the 4-dimensional behavior to a smaller functional form as ℓ becomes larger than $1/m$. In Figure 2.5, we graph the form of the mass term as a function of ℓ for the illustrative value $x = 0.3$.

There is another way to understand the behavior of the scalar mass term for $m\ell$ large. If m is large, we can consider the inner loop in Figure 2.4 to contract to a point. More precisely, because the function $P(k^2)$ is proportional to k^2 when k is small, this loop gives the pointlike operator $(-\nabla^2)$ acting on the two propagators which run from one wall to the other. The remaining one-loop integral may be evaluated in Euclidean coordinate space. There is one small subtlety to note. The representation of (2.19) in Euclidean coordinate space is

$$\left\langle a(x, x^5)a(y, y^5) \right\rangle = \frac{1}{8\pi^2} \sum_m \left(\frac{1}{[(x-y)^2 + (x^5 - y^5 + 2m\ell)^2]^{3/2}} \right.$$

$$\left. +P\frac{1}{[(x-y)^2 + (x^5 + y^5 + 2m\ell)^2]^{3/2}} \right) \ , \tag{2.57}$$

with m summed over all integers. When this expression is evaluated with one end at $x^5 = \ell$ and the other at $y^5 = 0$, we find (for $P = +1$)

$$\langle a(x, \ell)a(0, 0) \rangle = \frac{1}{8\pi^2} \sum_m \frac{2}{[x^2 + (2m + 1)^2\ell^2]^{3/2}} \ . \tag{2.58}$$

Then the evaluation of m_ϕ^2 involves the expression

$$I = \sum_{m,\tilde{m}} \int d^4x \frac{2}{8\pi^2[x^2 + (2m+1)^2\ell^2]^{3/2}}(-\nabla^2)\frac{2}{8\pi^2[x^2 + (2\tilde{m}+1)^2\ell^2]^{3/2}} , \qquad (2.59)$$

containing two propagators which run from a point 0 on the wall at $x^5 = 0$ to a point x on the wall at $x^5 = \ell$. By combining the two denominators with a Feynman parameter, it is not difficult to do the integral explicitly and then sum over m and $\tilde{m}$. The result is

$$I = \frac{3}{16\pi^2}\zeta(3)\frac{1}{\ell^4} . \qquad (2.60)$$

Multiplying this by the coefficient of k^2 in $P(k^2)$, we find again the result (2.56). This presentation explains the physical origin of the $1/\ell^4$ behavior of the diagrams.

2.5   Casimir energy

At the same time that supersymmetry breaking on the wall at $x^5 = \ell$ induces soft supersymmetry-breaking terms in other parts of the theory, it also creates a nonzero vacuum energy. We are particularly interested in the part of this energy which depends on ℓ—the Casimir energy [10]—since this term will eventually form a part of the balance which determines the physical value of ℓ. In this section, we will compute the Casimir energy due to the two mechanisms of supersymmetry breaking discussed in the previous section. We find it interesting that these calculations run almost in parallel to the calculations of the induced scalar mass term.

Consider first the case of a Fayet-Iliopoulos D-term on the boundary at $x^5 = \ell$. The coupling of this term to the bulk fields is described by the Lagrangian (2.31), plus a term proportional to $\delta(0)$ resulting from integrating out X^3. Since (2.31) is quadratic in Φ, we can integrate this field out explicitly. Using the propagator (2.33), the coupling of Φ to the boundary leads to

$$S_{eff} = \int d^5x\delta(x^5 - \ell) \cdot \frac{1}{2}\kappa\left(-\frac{g^2\kappa}{2\ell}\right) , \qquad (2.61)$$
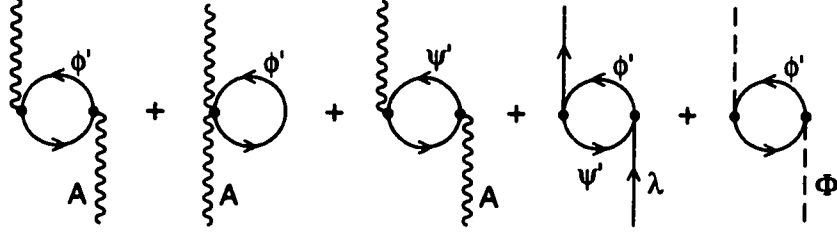
Figure 2.6: Feynman diagrams contributing to the Casimir energy due to loop effects of the supermultiplet on the wall at $x^5 = \ell$.

plus an ℓ-independent term proportional to $\delta(0)$. Thus, we find for the Casimir energy per 4-dimensional volume,

$$E_C/V_4 = +\frac{g^2\kappa^2}{4\ell} \ . \tag{2.62}$$

If there are D-terms on both boundaries, or if the fields ϕ_i on the two boundaries obtain expectation values as in (2.35), the sum of the two D terms appears in place of κ in (2.62). If the two D terms are equal and opposite, the Casimir energy vanishes. Also, as we observed already in (2.37), the $\delta(0)$ terms from integrating out X^3 and Φ precisely cancel. Thus, in this case, the vacuum energy remains just at zero, as expected from the supersymmetry of the situation.

In the case in which the spectrum at $x^5 = \ell$ violates supersymmetry but there is no induced D term, the Casimir energy must be generated by radiative corrections. The leading contribution comes from the diagrams shown in Figure 2.6. These diagrams involve a closed loop on the boundary at $x^5 = \ell$ and a propagator from the 5-dimensional Yang-Mills theory which winds around the compactified direction.

Though perhaps it is not completely obvious from the beginning, the structure of the diagrams in Figure 2.6 is very similar to that of the diagrams in Figure 2.3. As in the previous section, we will describe the calculation for the case $\mathrm{str}[M^2] = 0$.

In the diagrams of Figure 2.6, we have only one sum over k^5. Thus, define for this section

$$[\mathcal{B}] = \frac{1}{2\ell}\sum_n \mathcal{B}(k^5) \ . \tag{2.63}$$

Then the Casimir energy resulting from this set of diagrams can be written in terms of Euclidean scalar two-loop integrals as

$$E_C/V_4 = \frac{1}{2}g^2 d_G C(R')[k^2 \mathcal{R}_C + 4\mathcal{S}_C] \,, \tag{2.64}$$

where $d_G C(R') = \text{tr}_{R'}[t^A t^A]$, and

$$
\begin{aligned}
\mathcal{R}_C &= (k^5|m_+|m_+) + (k^5|m_-|m_-) + 2(k^5|m_+|m_-) + 4(k^5|m|m) \\
&\quad -4(k^5|m_+|m) - 4(k^5|m_-|m) \\
\mathcal{S}_C &= m_+^2 \left\{ (k^5|m_+|m_+) - (k^5|m_+|m) \right\} - m^2 \left\{ (k^5|m|m) - (k^5|m_+|m) \right\} \\
&\quad m_-^2 \left\{ (k^5|m_-|m_-) - (k^5|m_-|m) \right\} - m^2 \left\{ (k^5|m|m) - (k^5|m_-|m) \right\} \quad (2.65)
\end{aligned}
$$

The inner loop of each of these two-loop integrals can be evaluated explicitly, giving the same functions $R(k^2)$, $S(k^2)$, $P(k^2)$ that we saw earlier in (2.49) and (2.50).

Again we can simplify the sum over k^5 using the contour trick from finite temperature field theory. Write

$$\frac{1}{2\ell} \sum_n \frac{1}{k^2 + (k^5)^2} = \oint \frac{dk^5}{2\pi} \frac{1}{e^{2ik^5\ell} - 1} \frac{1}{k^2 + (k^5)^2} \,, \tag{2.66}$$

where the contour encloses the poles of the integrand at $k^5 = \pi n/\ell$. Draw the contour as a line from left to right just below the real axis and another line from right to left just above this axis. Push the first line down and pick up the pole at $k^5 = -ik$. For the contour integral on the line above the axis, replace

$$\frac{1}{e^{2ik^5\ell} - 1} = -1 - \frac{1}{e^{-2ik^5\ell} - 1} \,. \tag{2.67}$$

In the second term, push the contour up and pick up the pole at $k^5 = ik$. These manipulations convert (2.66) to the form

$$\frac{1}{k} \frac{1}{e^{2k\ell} - 1} + \int_{-\infty}^{\infty} \frac{dk^5}{(2\pi)} \,. \tag{2.68}$$

The second term in (2.68) is independent of ℓ; it represents the contribution to the

vacuum energy of the 4-dimensional wall in an infinite 5-dimensional volume. Equivalently, from the point of view of propagators in coordinate space, this term is the contribution of the propagators that go from the wall back to the wall without winding around x^5. In any event, this term does not contribute to the Casimir energy, and we may drop it.

After these manipulations, the Casimir energy (2.64) takes the form

$$E_C/V_4 = -\frac{1}{2}\left(\frac{g^2}{(4\pi)^4}\right) d_G C(R') \int_0^\infty dk k^2 \frac{1}{e^{2k\ell}-1} P(k^2) , \qquad (2.69)$$

where $P(k^2)$ is the same field strength renormalization function that appeared in (2.51).

As in the previous section, we can analyze the two-loop integral in the limits of small and large ℓ. Consider first the limit $\ell \to 0$. If we formally take the limit of small ℓ in (2.69), we obtain a divergent integral

$$E_C/V_4 \sim -\int_0^\infty dk \frac{k}{\ell}\frac{1}{k^2} \log k^2 . \qquad (2.70)$$

Thus, unlike the case of m_ϕ^2, the contributions to the Casimir energy are dominated by large values of k^2. The estimate

$$\int_0^\infty dk k^2 \frac{1}{e^{2k\ell}-1}\frac{1}{k^2} \log k^2 \sim \frac{1}{2\ell}\log^2\frac{1}{m\ell} \qquad (2.71)$$

and the asymptotic formula for $P(k^2)$ given in the Appendix gives a precise formula for the small ℓ behavior:

$$E_C/V_4 = -\frac{1}{2}\left(\frac{g^2}{(4\pi)^4}\right) d_G C(R') \cdot \frac{4m^4 x^2}{\ell}\log^2\frac{1}{m\ell} . \qquad (2.72)$$

For large ℓ, the analysis can be done along the same lines as those we used for m_ϕ^2. The denominator of (2.69) cuts off the integrand for all but small k^2. Thus, we can replace $P(k)$ by its leading term as $k^2 \to 0$. With this approximation, the integral is
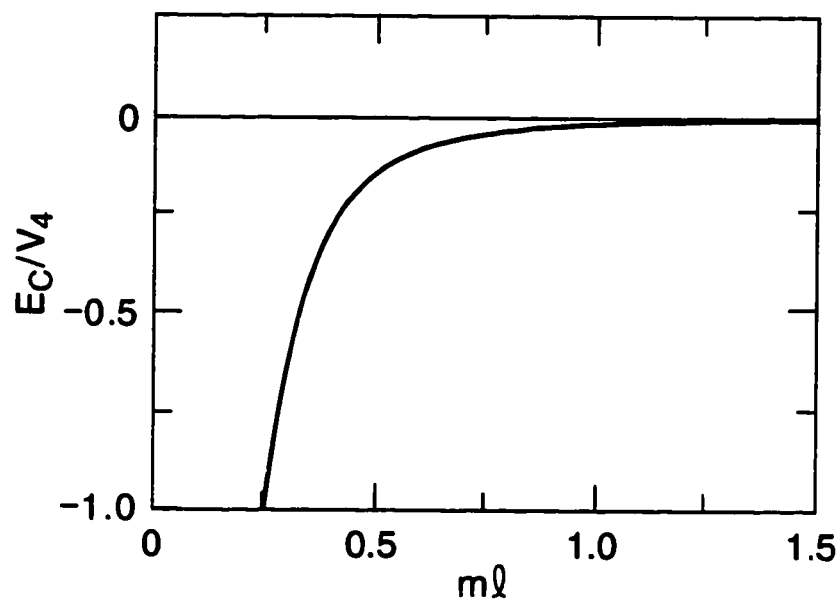
(E_C/V_4) is plotted in units of $\frac{1}{2}d_G C(R')(g^2/(4\pi)^4))$.

Figure 2.7: Behavior of the Casimir energy as a function of ℓ.

easily evaluated, and we obtain

$$
\begin{aligned}
E_C/V_4 = -\frac{1}{2}\left(\frac{g^2}{(4\pi)^4}\right) d_G C(R')\zeta(5)\frac{1}{\ell^5} \\
\left\{\frac{3}{2}\left[\frac{4+x-2x^2}{x^2}\log(1+x) - \frac{4-x}{x}\right] + (x \leftrightarrow -x)\right\} .
\end{aligned}
\tag{2.73}
$$

Comparing (2.72) and (2.73), we see the same crossover that we found previously from (2.55) to (2.56). In Figure 2.7, we graph the form of the Casimir energy as a function of ℓ for the illustrative value $x = 0.3$.

As in the previous section, the behavior of the Casimir energy for large ℓ is studied most easily in Euclidean coordinate space. If ℓ or m is large, the inner loop of each two-loop diagram can be contracted to a local operator proportional to $(-\nabla^2)$. Then the Casimir energy is proportional to an expression in which this operator acts on a propagator which runs around the compact direction. More specifically, the Casimir energy is proportional to

$$
J = \sum_m (-\nabla^2)\frac{1}{8\pi^2(x^2 + (m\ell)^2)^{3/2}}\bigg|_{x=0} ,
\tag{2.74}
$$

where the sum over m runs over all integers except $m = 0$. This expression evaluates to

$$
J = \frac{3}{32\pi^2}\zeta(5)\frac{1}{\ell^5} .
\tag{2.75}
$$

Multiplying this by the coefficient of k^2 in $P(k^2)$, we return to the result (2.73).

Both of the individual contributions to the Casimir energy that we found in this section are monotonic in ℓ. We find it interesting, though, that these two contributions have opposite signs. Thus, it is possible that, in a realistic theory, we could find balancing contributions to the Casimir energy that stabilize the value of ℓ at a nonzero value.

2.6   Hořava's supersymmetry-breaking structure

Now that we have analyzed mechanisms for supersymmetry breaking in our toy model, it is interesting to ask whether this sheds light on the mechanism of supersymmetry breaking in string theory proposed by Hořava [8]. We can see the connection by making a dimensional reduction of Hořava's system from 11 to 5 dimensions, taking the compact 6 dimensions to be a Calabi-Yau manifold. Under this reduction, the boundary gaugino condensate becomes a 4-dimensional scalar gaugino bilinear on the boundary. The relevant components of the 3-form gauge field in the bulk are those that multiply the the (3,0) or (0,3) forms of the Calabi-Yau space,

$$C_{ABC}(x, x^5, y) = c(x, x^5)\Omega_{ABC}(y) + \cdots \qquad (2.76)$$

These components form two complex 5-dimensional fields which belong to a hyper-multiplet in the bulk. Thus, we can try to recover Hořava's coupling of the bulk and boundary fields by considering the coupling of a hypermultiplet in the bulk to chiral fields on the boundary.

We can analyze this problem using arguments similar to those in Section 2. The five-dimensional hypermultiplet consists of a pair of complex scalars A^i, a Dirac fermion χ, and a pair of complex auxiliary fields F^i. Under supersymmetry they transform as follows [24]:

$$
\begin{aligned}
\delta_\xi A^i &= -\sqrt{2}\epsilon^{ij}\bar{\xi}^j\chi \\
\delta_\xi \chi &= +\sqrt{2}i\gamma^M\partial_M A^i\epsilon^{ij}\xi^j + \sqrt{2}F^i\xi^i \\
\delta_\xi F^i &= -\sqrt{2}i\bar{\xi}^i\gamma^M\partial_M\chi \ .
\end{aligned} \qquad (2.77)
$$

To carry out the orbifold projection, we must consistently assign parities P to the various fields and impose the boundary conditions (2.10). Here is a consistent set of

assignments which gives $N = 1$ supersymmetry on the wall:

	$P = +1$	$P = -1$
ξ	ξ_L^1	ξ_L^2
A^i	A^1	A^2
χ	χ_L	χ_R
F^i	F^1	F^2

$$(2.78)$$

As in Section 2, we project out the odd-parity states and consider the supersymmetry on the boundary generated by ξ_L^1. The transformations (2.77) specialize to

$$
\begin{aligned}
\delta_\xi A^1 &= \sqrt{2}\xi_L^{1T}\chi_L \\
\delta_\xi \chi_L &= \sqrt{2}i\sigma^m\partial_m A^1\xi_L^{1*} - \sqrt{2}\partial_5 A^2\xi_L^1 + \sqrt{2}F^1\xi_L^1 \\
\delta_\xi F^1 &= i\sqrt{2}\xi_L^{1\dagger}\bar{\sigma}^m\partial_m\chi_L + \sqrt{2}\xi_L^{1\dagger}\partial_5\chi_R \\
\delta_\xi\partial_5 A^2 &= \sqrt{2}\xi_L^{1\dagger}\partial_5\chi_R \ .
\end{aligned}
$$

$$(2.79)$$

These transformations imply that

$$
\delta_\xi(F^1 - \partial_5 A^2) = \sqrt{2}i\xi_L^{1\dagger}\bar{\sigma}^m\partial_m\chi_L \ ,
$$

$$(2.80)$$

Then A^1, χ_L, $(F^1 - \partial_5 A^2)$ transform as the complex scalar, chiral fermion, and auxiliary field components of a four-dimensional $N = 1$ chiral multiplet.

We can use this set of fields to write a coupling of the bulk hypermultiplet to chiral superfields on the boundary. In particular, the boundary theory might have a superpotential which depends on the boundary chiral fields ϕ_i and the boundary value of the field A^1. The superpotential term then includes the boundary action

$$
\mathcal{L}_4 = (F^1 - \partial_5 A^2)\frac{\partial W}{\partial A^1} + \cdots \ .
$$

$$(2.81)$$

If we integrate out the auxiliary field F^1 and write the resulting action in 5 dimensions,

we arrive at the structure

$$\mathcal{L}_5 = |\partial_M A^2|^2 - \delta(x^5) \left[\partial_5 A^2 \frac{dW}{dA^1} + h.c. \right] + (\delta(x^5))^2 \left| \frac{dW}{dA^1} \right|^2 \qquad (2.82)$$

If we identify A^2 with the scalar component of C_{ABC} shown in (2.76) and (dW/dA^1) with the E_8 gaugino condensate, this reproduces the perfect-square structure (2.1) found by Hořava [6, 8].

From here, we could go on to discuss the communication of supersymmetry breaking. If we simply assume a fixed value of the gaugino condensate and solve for A^2 as in (2.33), we find a universal gaugino mass proportional to $1/\ell$, as in [14, 15, 16]. This leads to conventional supergravity-mediated supersymmetry breaking scenario. It would be very interesting to know whether there are other possibilities. In particular, it would be interesting to find a perturbative hierarchy of soft supersymmetry-breaking terms similar to the one that we discussed in Section 4. To search for such possibilities, it is necessary to understand the general coupling of boundary matter fields to supergravity.

2.7   Conclusion

In this chapter, we have shown how easy it is to construct consistent couplings of five-dimensional supermultiplets to matter multiplets on orbifold walls by analyzing the transformation properties of the associated auxiliary fields. We applied this method to some simple models with bulk and boundary fields and exhibited several possibilities for the communication of supersymmetry breaking from one wall to the other. We hope that this method will generalize to supergravity and allow a more complete understanding of the supersymmetry breaking and its phenomenology in the Hořava-Witten approach to unification.

2.8 Appendix:

More about the two-loop self-energy

In this appendix, we will give some further details of the two-loop self-energy calculations discussed in Sections 3 and 4.

As we explained in (2.27), our strategy for computing the diagrams shown in Figure 2.3 began with bringing each diagram into the form

$$
\begin{aligned}
M^2 &= -g^4 C_2(R) C(R') \\
&\times \int_q \int_{k55} \frac{N(k, k^5, \hat{k}^5, q)}{(k^2)(k^2 - (k^5)^2)(k^2 - (\hat{k}^5)^2)(q^2 - m_1^2)((q - k)^2 - m_2^2)}
\end{aligned} \tag{2.83}
$$

for the m_1, m_2 appropriate to the inner loop of the diagram. We now give the contributions of the various diagrams to the numerator polynomial N. In the following formula, we write the contributions to N as a sum, following the order of the diagrams in Figure 2.3, although properly each separate term should receive the appropriate particle masses in the denominator. The expression is given for the mass spectrum (2.40) considered in Section 4; for the analysis of Section 3, one should set all masses equal to zero. With this explanation,

$$
\begin{aligned}
N &= 2(k \cdot (2q - k))^2 - 2(q^2 - m_+^2 + q^2 - m_-^2)k^2 - 2(2q - k)^2 k^2 \\
&\quad + 8(q^2 - m_+^2 + q^2 - m_-^2)k^2 \\
&\quad + 4(q \cdot (q - k)k^2 - 2q \cdot k(q - k) \cdot k - m^2 k^2) \\
&\quad - 8k^2(q \cdot (q - k) - 2m^2) + 16k^2 k \cdot (q - k) + 2k^2 + 0 + 0 .
\end{aligned} \tag{2.84}
$$

If we set all masses equal to zero, this expression vanishes after the use of the $q \leftrightarrow (k - q)$ symmetry of the denominator. With nonzero masses, some simple rearrangements and a Euclidean rotation bring the expression for m_ϕ^2 into the form (2.44).

In our analysis of (2.44), we made use of the self-energy integral $b(k^2, m_1^2, m_2^2)$

defined by (2.48). We can write b more explicitly as

$$
\begin{aligned}
b(k^2, m_1^2, m_2^2) &= \int_0^\infty dx \log\left(x(1-x)k^2 + xm_1^2 + (1-x)m_2^2\right) \\
&= A \log\left[\frac{(A+B_1)(A+B_2)}{(A-B_1)(A-B_2)}\right] \\
&\quad + B_2 \log m_1^2 + B_1 \log m_2^2 - 2 ,
\end{aligned}
\tag{2.85}
$$

where

$$
A = \left[\frac{k^4 + 2k^2(m_1^2 + m_2^2) + (m_1^2 - m_2^2)^2}{4k^4}\right]^{1/2}
\tag{2.86}
$$

and

$$
B_1 = \frac{k^2 + m_1^2 - m_2^2}{2k^2} , \qquad B_2 = \frac{k^2 + m_2^2 - m_1^2}{2k^2} .
\tag{2.87}
$$

From $b(k^2, m_1^2, m_2^2)$, we can compute the combinations $R(k^2)$, $S(k^2)$, $P(k^2)$ defined in (2.49) and (2.51). We evaluate these expressions using the mass spectrum derived from (2.40). It is straightforward to work out the asymptotic behavior of these functions for large and small values of k^2. For $P(k^2)$, we find, as $m^2k^2 \to 0$,

$$
P(k^2) = k^2 \left[\frac{4 + x - 2x^2}{x^2} \log(1+x) + 1 + (x \leftrightarrow -x)\right] + \mathcal{O}(k^4) .
\tag{2.88}
$$

and as $m^2k^2 \to \infty$,

$$
\begin{aligned}
P(k^2) &= \frac{4m^4}{k^2}\left[x^2 \log \frac{k^2}{m^2} - (x^2 + 3x + 2)\log(1+x) - x^2 + (x \leftrightarrow -x)\right] \\
&\quad + \mathcal{O}(k^{-4}) .
\end{aligned}
\tag{2.89}
$$

The computation of the Casimir energy reported in Section 5 is very similar to the computation of m_ϕ^2 and, in particular, uses the same auxiliary function $P(k^2)$.

Chapter 3

Emission of Gravitons into Extra Dimensions

Recently, Arkani-Hamed, Dimopoulos, and Dvali have proposed that there are extra compact dimensions of space, accessible to gravity but not to ordinary matter, which could be macroscopically large. In this chapter, we derive the effective coupling between ordinary matter and higher-dimensional gravitons, and compute various cross sections to produce extra-dimensional gravitons in particle collisions. We argue that high-energy collider processes in which gravitons are radiated into these new dimensions place significant, model-independent constraints on this picture, and we present the constraints from anomalous single photon production at e^+e^- colliders and from monojet production at hadron colliders.

3.1   Introduction

The Standard Model of strong, weak, and electromagnetic interactions has been dramatically successful in explaining the rates of high-energy e^+e^- and $p\bar{p}$ reactions and the properties of the W and Z bosons. This great success, however, has focused attention on the fact the Standard Model (SM) requires a number of choices for its input parameters which are very difficult to understand. Among these are the value of the Higgs boson mass parameter μ^2 and the value of the cosmological constant

λ. If one assumes that the most fundamental scale in Nature is the Planck scale, $M_{Planck} = G_N^{-1/2} = 10^{19}$ GeV and writes these parameters in terms of this scale, one finds $\mu^2 \sim 10^{-34} M_{Planck}^2$, $\lambda \sim 10^{-116} M_{Planck}^4$.

The mystery of these small parameters has motivated many authors to consider radical ideas for the manner in which gravity is unified with the other fundamental interactions. The introduction of supersymmetry can lower the natural mass scale for μ^2 and λ to 1 TeV. This ameliorates the problem of the Higgs mass but is not nearly enough of a reduction to solve the cosmological constant problem. Many authors have investigated whether a string theory of quantum gravity can provide a further reduction. String theory includes the possibility of additional microscopic space dimensions. In this context, Antoniadis [32] has proposed that Nature may contain additional compact dimensions of size $\hbar/$TeV [33].

Recently, several groups [34, 35, 36] have extended this proposal using new ideas about the strong-coupling behavior of string theory. In this regime, string theory may contain solitons or mirror surfaces that occupy lower-dimensional hypersurfaces, with some species of particle restricted to these objects. One can then imagine that the quarks, leptons, and gauge bosons of the SM live on a 4-dimensional hypersurface inside the full space-time, while gravity lives in the full, higher-dimensional space. Arkani-Hamed, Dimopoulos, and Dvali (ADD) [35] have argued that, in these models, the fundamental gravitational scale can be as low as TeV energies, while the size of the extra dimensions can be as large as a millimeter.

If indeed gravity becomes strong at TeV energies, gravitons should be radiated at significant rates in high-energy particle collisions. In collider experiments, higher-dimensional gravitons (G) appear as massive spin-2 neutral particles which are not observed by collider detectors. As ADD pointed out, G radiation leads to missing-energy signatures in which a photon or a jet is produced with no observable particle balancing its transverse momentum.

In this chapter, we calculate the cross section for emitting a real graviton off of the four-dimensional membrane into the extra-dimensional bulk. We begin in section 3.2 with a summary of the scenario proposed by Arkani-Hamed, Dimopoulos, and Dvali in [35]. In section 3.3 we describe the interaction of the Standard Model (SM)

particles with the extra-dimensional gravitons in this scenario, and in section 3.4 we calculate the cross sections for the processes gluon + gluon → gluon + graviton and quark + antiquark → gluon + graviton. In section 3.5 we present some expected signals at current and future lepton and hadron colliders from the processes $e^+e^- \to$ $\gamma +$ (missing) and $p\bar{p} \to$ jet + (missing) and briefly conclude in section 3.6. Section 3.7 contains a brief discussion of the gravity-fermion coupling used, and 3.8 gives the expressions for center-of-mass momenta and polarizations used in calculating matrix elements and polarizations sums.

3.2 The Large Extra Dimension Scenario

In this section we summarize the scenario of Arkani-Hamed, Dimopoulos, and Dvali described in [35]. They begin by supposing that there are n extra spatial dimensions compactified to a volume R^n. For distances r much smaller than the compactification scale R the gravitational potential has behavior characteristic of a $(4+n)$-dimensional space:

$$V(r) \sim \left(\frac{m_1 m_2}{M_{fund}^{n+2}}\right) \frac{1}{r^{n+1}}, \qquad (r \ll R), \tag{3.1}$$

where M_{fund} is the fundamental scale setting the strength of the higher-dimensional gravitational force. For large distances $r \gg R$ the compact dimensions can be ignored (except for their use in relating large-distance potentials to the short-distance scale M_{fund}) and the potential has behavior characteristic of a 4-dimensional space:

$$V(r) \sim \left(\frac{m_1 m_2}{M_{fund}^{n+2} R^n}\right) \frac{1}{r}, \qquad (r \gg R). \tag{3.2}$$

For this to agree with the familiar large-distance behavior of the potential given by:

$$V(r) \sim \left(\frac{m_1 m_2}{M_{Planck}^2}\right) \frac{1}{r}, \tag{3.3}$$

we must have:

$$M_{fund}^{n+2} R^n \approx M_{Planck}^2, \tag{3.4}$$

or:

$$R \sim M_{fund}^{-1} \left(\frac{M_{Planck}^2}{M_{fund}^2} \right)^{1/n}. \tag{3.5}$$

Note that for an arbitrary ratio between the fundamental scale M_{fund} and the four dimensional Planck scale M_{Planck}, the required compactification radius approaches the fundamental length scale M_{fund} as the number of extra dimensions is taken to infinity. The authors of [35] then assume there is no hierarchy between the fundamental high-energy physics scale M_{fund} and the electroweak scale. This single scale sets the strength of both the electroweak force and (higher-dimensional) gravity. Using $M_{fund} \approx 1\ TeV$ gives:

$$R \approx 10^{\frac{34}{n} - 20}\ \text{meters}. \tag{3.6}$$

A model with one extra dimension ($n = 1$) would have a compactification scale R on the order of the size of the solar system, leading to scaling for the potential $V \sim 1/r^2$ at planetary scales which is grossly excluded. However, for two extra dimensions the compactification scale is roughly a millimeter, and direct measurements of gravity at this scale have not yet been performed[37, 38].

In contrast to gravitational physics, SM gauge physics has been explored up to roughly the electroweak scale with no observed deviations from the expected four-dimensional behavior, and so matter and gauge forces must be confined to a four-dimensional membrane with an extra-dimensional volume no larger than this scale (which we might expect if the membrane comes from dynamics characterized by the scale $M_{fund} \approx 1\ TeV$). Only gravitational (and, potentially, new non-standard-model) fields are allowed to propagate in the bulk. Although gauge and matter fields can be localized on a membrane through nonperturbative string/M dynamics, the authors of [35] point out that field theoretic effects can also be used to achieve such a localization. We remain agnostic concerning the detailed dynamics confining the SM fields to the membrane, and study the scenario in a model-independent fashion based on an effective field theory.

Even with the confinement of the standard model particles to a four-dimensional membrane, one still has to worry about non-observation of new physics signals at high energies, as this new model predicts that the usual weakness of the gravitational

coupling disappears at energies close to the electroweak scale. The authors of [35] present an order-of-magnitude estimate of the cross section for emission of gravitons off of the four-dimensional membrane and into the bulk. They estimate that the effective four-dimensional cross section to produce an individual graviton should be $\sim 1/M^2_{Planck}$ based on dimensional analysis, and reactions at an energy scale E can produce any of the $(ER)^n$ Kaluza-Klein excitations of the graviton with a mass below E, so the total cross section is roughly $(ER)^n/M^2_{Planck}$. Using the relation of equation 3.5 makes this cross section $\sim E^n/M^{2+n}_{fund}$.

3.3 Graviton Interactions

In this section, we determine the interactions between the SM particles and the gravitons in the extra dimensions. We remain uncommitted to any particular underlying dynamics and ignore the possibility of additional model-dependent bulk fields[1]. We will also assume that the four-dimensional manifold is flat and of negligible thickness and that the energies required to excite fluctuations of the four dimensional membrane itself are larger than the energy scales under examination, so that such fluctuations can be ignored. We will further assume that the deviation of the higher-dimensional background metric due to the presence of the membrane is negligible. For definiteness, we will assume that the n extra dimensions are compactified on an n-dimensional torus of periodicity $2\pi R$.

Coordinate invariance dictates the form of the couplings of the graviton to SM particles on the membrane, which may be derived in the familiar manner by writing a covariant SM Lagrangian on a manifold using the induced metric on that manifold, and then introducing the graviton field as the difference between the full metric and a flat-space background: $g_{MN} = \eta_{MN} + \lambda h_{MN}$ (where $\lambda = 2\sqrt{8\pi G_{Newt}}$ for four-dimensional graviton normalization) as is done by Sundrum in [39]. Fermion couplings require tetrads e^a_μ and spin connections ω^{ab}_μ consistent with the induced metric on the four dimensional membrane. Although Sundrum provides a method of construction of

---

[1]These fields would presumably couple with gravitational strength and would produce additional, model-dependent, missing-energy signatures beyond those we consider here.

these entities in terms of explicit frame rotations along the four-dimensional manifold, one may use the simplified strategy described appendix A of this chapter (section 3.7) if the intrinsic curvature of the membrane is perturbatively small.

If one restricts attention to interactions which are first-order in the gravitational coupling λ, one may use the elegant coupling term:

$$S_{int} = -\int d^4x \frac{\lambda}{2} h_{\mu\nu} T_{SM}^{\mu\nu}, \tag{3.7}$$

(where $T_{SM}^{\mu\nu}$ is the flat-space four-dimensional stress-energy tensor of the Standard Model). This equation may be derived in the above framework by simply writing:

$$S(g_{\mu\nu}) = S(\eta_{\mu\nu}) + \lambda h_{\mu\nu} \left(\frac{\delta S_{SM}}{\delta g_{\mu\nu}} \right) + O(\lambda^2), \tag{3.8}$$

and using the definition of the stress-energy tensor:

$$T_{SM}^{\mu\nu} = \frac{1}{2} \frac{\delta S_{SM}}{\delta g_{\mu\nu}} \tag{3.9}$$

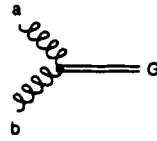(where $S_{SM} = \int d^4x \sqrt{-det(g_{\mu\nu})} \mathcal{L}_{SM}$ is the Standard Model action).

This leads to the following interaction Lagrangian for a graviton $h_{\mu\nu}$, a gauge field A_μ^a and a chiral fermion ψ:

$$
\begin{aligned}
\mathcal{L}_{int} = & \ \mathcal{L}_{int(SM)} \\
& + \frac{\lambda}{2} h_{\mu\nu} \left(F_{\mu\alpha}^a F_{\nu\beta}^a \eta^{\alpha\beta} - \frac{1}{4} \eta_{\mu\nu} F_{\alpha\beta}^a F_{\alpha'\beta'}^a \eta^{\alpha\alpha'} \eta^{\beta\beta'} \right) \\
& + \frac{\lambda}{2} h_{\mu\nu} \left(\psi \frac{[\bar{\sigma}^\mu D^\nu - \eta^{\mu\nu} \bar{\sigma}^\rho D_\rho]}{2} \psi + h.c. \right),
\end{aligned} \tag{3.10}
$$
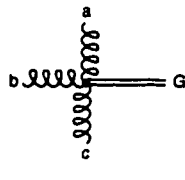
where $F_{\mu\nu}^a \equiv \partial_\mu A_\nu^a - \partial_\nu A_\mu^a + g f^{abc} A_\mu^b A_\nu^c$ and $D_\mu \equiv \partial_\mu \otimes 1 - ig A_\mu^a \otimes t^a$. By inspection, this gives the interaction vertices displayed in figure 3.1. Note that when coupling to spin-2 gravitons $h_{\mu\nu}$ in the traceless gauge we can ignore the terms $\sim \eta^{\mu\nu}$.

The interaction Lagrangian of equation (3.10) provides the same coupling as in ordinary four-dimensional gravity—the difference between the scenario we discuss and

Vertices defined with inward momenta. All vertices should be symmetrized on μ and ν or projected onto symmetric polarization states $\epsilon_{\mu\nu}^{(G)}$.

$$= \quad i\lambda[(p^{(a)} \cdot p^{(b)})\eta^{\alpha\mu}\eta^{\beta\nu} + \eta^{\alpha\beta}p^{(a)\mu}p^{(b)\nu}$$
$$- \eta^{\beta\nu}p^{(a)\mu}p^{(b)\alpha} - \eta^{\alpha\mu}p^{(a)\beta}p^{(b)\nu}]\epsilon_\alpha^{(a)}\epsilon_\beta^{(b)}\epsilon_{\mu\nu}^{(G)}\delta_{AB}$$
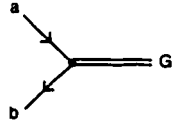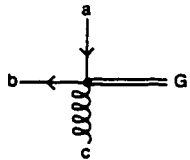
$$= \quad -\lambda g[p_\beta^{(a)}\eta_{\gamma\mu}\eta_{\alpha\nu} - \eta_{\alpha\beta}\eta_{\gamma\mu}p_\nu^{(a)}$$
$$+ p_\gamma^{(b)}\eta_{\alpha\mu}\eta_{\beta\nu} - \eta_{\beta\gamma}\eta_{\alpha\mu}p_\nu^{(b)} + p_\alpha^{(c)}\eta_{\beta\mu}\eta_{\gamma\nu} - \eta_{\gamma\alpha}\eta_{\beta\mu}p_\nu^{(c)}$$
$$- p_\gamma^{(a)}\eta_{\beta\mu}\eta_{\alpha\nu} + \eta_{\alpha\gamma}\eta_{\beta\mu}p_\nu^{(a)} - p_\alpha^{(b)}\eta_{\gamma\mu}\eta_{\beta\nu} + \eta_{\beta\alpha}\eta_{\gamma\mu}p_\nu^{(b)}$$
$$- p_\beta^{(c)}\eta_{\alpha\mu}\eta_{\gamma\nu} + \eta_{\gamma\beta}\eta_{\alpha\mu}p_\nu^{(c)}]\epsilon_\alpha^{(a)}\epsilon_\beta^{(b)}\epsilon_\gamma^{(c)}\epsilon_{\mu\nu}^{(G)}$$

$$= \quad \frac{-i\lambda}{4}u^{(b)\dagger}[\bar\sigma^\mu(p^{(a)} + p^{(b)})^\nu]u^{(a)}\epsilon_{\mu\nu}^{(G)}\delta_{AB}$$

$$= \quad \frac{-i\lambda}{2}gt_{AB}^c u^{(b)\dagger}[\bar\sigma^\mu\eta^{\gamma\nu}]u^{(a)}\epsilon_{\mu\nu}^{(G)}\epsilon_\gamma^{(c)}$$

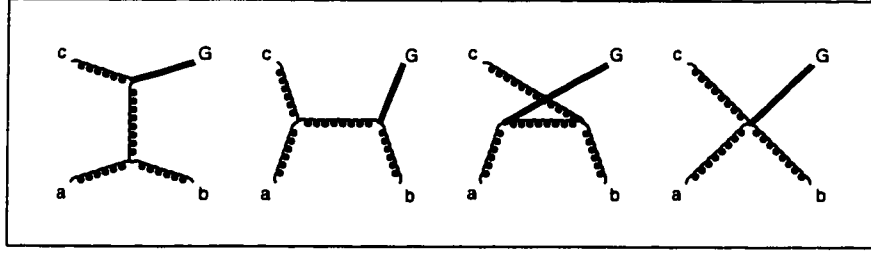Figure 3.1: Interaction vertices between Kaluza-Klein graviton modes and Standard Model particles.

Figure 3.2: Feynman diagrams contributing to the process $gg \to gG$.

standard gravitational physics is that there is a Kaluza-Klein tower of massive spin-2 gravitons with this coupling.

The propagation of the higher-dimensional gravitons may be treated through four-dimensional methods by summing over their Kaluza-Klein modes. In a four-dimensional description, the sum over graviton momenta in the compact directions becomes a sum over gravitons with Kaluza-Klein masses related to the momentum in the n extra dimensions by $m^2 = \sum_{i=4+1}^{4+n} k_i^2$. For processes involving many such modes, we can replace this sum with an integral:

$$
\begin{aligned}
\sum_m &= R^n \int d^n m \\
&= \frac{1}{2}\Omega_n R^n \int (m^2)^{(n-2)/2} dm^2 \\
&= \frac{\Omega_n}{8\pi} M^{-(n+2)} \int (m^2)^{(n-2)/2} dm^2 \, G_N^{-1} \,,
\end{aligned}
\tag{3.11}
$$

where Ω_n is the volume of the unit sphere in n dimensions ($= 2\pi$ for $n = 2$).

3.4 Calculation of $gg \to gG$ and $q\bar{q} \to \mathbf{gG}$

In this section, we calculate the cross sections for the processes gluon + gluon $\to$ gluon + graviton and quark + antiquark $\to$ gluon + graviton in the context of the large extra dimension scenario.

The Feynman diagrams for the process $gg \to gG$ are displayed in figure 3.2. Using

the interaction rules from figure 3.1 and using the conditions:

$$p^{(a)} \cdot \epsilon^{(a)} = p^{(b)} \cdot \epsilon^{(b)} = k^{(c)} \cdot \epsilon^{(c)} = k^{(G)\mu} \epsilon^{(G)}_{\mu\nu} = \eta^{\mu\nu} \epsilon^{(G)}_{\mu\nu} = 0, \qquad (3.12)$$

leads to the following expression for the amplitude for a gluon with 4-momentum $p^{(a)}$, polarization vector $\epsilon^{(a)}$ and color a and a gluon with 4-momentum $p^{(b)}$, polarization vector $\epsilon^{(b)}$ and color b to scatter into a gluon with 4-momentum $k^{(c)}$, polarization vector $\epsilon^{(c)}$ and color c and a graviton with 4-momentum $k^{(G)}$ and polarization tensor $\epsilon^{(G)}$:

$$\mathcal{A}^{abc} = \lambda g f^{abc} \left(\mathcal{A}^{(1)}_{\alpha\beta\gamma\mu\nu} + \mathcal{A}^{(2)}_{\alpha\beta\gamma\mu\nu} + \mathcal{A}^{(3)}_{\alpha\beta\gamma\mu\nu} + \mathcal{A}^{(4)}_{\alpha\beta\gamma\mu\nu} \right) \epsilon^{(a)\alpha} \epsilon^{(b)\beta} \epsilon^{(c)\gamma} \epsilon^{(G)\mu\nu}, \qquad (3.13)$$

where we have:

$$\mathcal{A}^{(1)}_{\alpha\beta\gamma\mu\nu} = \frac{1}{s} \left(\eta_{\alpha\beta}(p^{(a)}_\chi - p^{(b)}_\chi) + 2\eta_{\beta\chi} p^{(b)}_\alpha - 2\eta_{\chi\alpha} p^{(a)}_\beta \right) \qquad (3.14)$$
$$\left(-(k^{(c)} \cdot k^{(G)}) \eta_{\gamma\mu} \eta_{\chi\nu} - \eta_{\gamma\chi} k^{(c)}_\mu k^{(c)}_\nu + k^{(G)}_\gamma k^{(c)}_\mu \eta_{\chi\nu} + k^{(c)}_\chi \eta_{\gamma\mu} k^{(c)}_\nu \right)$$

$$\mathcal{A}^{(2)}_{\alpha\beta\gamma\mu\nu} = \frac{1}{t} \left(2\eta_{\alpha\chi} p^{(a)}_\gamma + 2\eta_{\chi\gamma} k^{(c)}_\alpha + \eta_{\gamma\alpha}(-k^{(c)}_\chi - p^{(a)}_\chi) \right) \qquad (3.15)$$
$$\left((p^{(b)} \cdot k^{(G)}) \eta_{\chi\mu} \eta_{\beta\nu} - \eta_{\chi\beta} p^{(b)}_\mu p^{(b)}_\nu + p^{(b)}_\chi p^{(b)}_\mu \eta_{\beta\nu} - k^{(G)}_\beta \eta_{\chi\mu} p^{(b)}_\nu \right)$$

$$\mathcal{A}^{(3)}_{\alpha\beta\gamma\mu\nu} = \frac{1}{u} \left(-2\eta_{\chi\beta} p^{(b)}_\gamma + \eta_{\beta\gamma}(p^{(b)}_\chi + k^{(c)}_\chi) - 2\eta_{\gamma\chi} k^{(c)}_\beta \right) \qquad (3.16)$$
$$\left((p^{(a)} \cdot k^{(G)}) \eta_{\alpha\mu} \eta_{\chi\nu} - \eta_{\alpha\chi} p^{(a)}_\mu p^{(a)}_\nu - k^{(G)}_\alpha p^{(a)}_\mu \eta_{\chi\nu} + p^{(a)}_\chi \eta_{\alpha\mu} p^{(a)}_\nu \right)$$

$$\mathcal{A}^{(4)}_{\alpha\beta\gamma\mu\nu} = (-1)(p^{(a)}_\beta \eta_{\gamma\mu} \eta_{\alpha\nu} - \eta_{\alpha\beta} \eta_{\gamma\mu} p^{(a)}_\nu \qquad (3.17)$$
$$+ p^{(b)}_\gamma \eta_{\alpha\mu} \eta_{\beta\nu} - \eta_{\beta\gamma} \eta_{\alpha\mu} p^{(b)}_\nu$$
$$+ (-k^{(c)}_\alpha) \eta_{\beta\mu} \eta_{\gamma\nu} - \eta_{\gamma\alpha} \eta_{\beta\mu} (-k^{(c)}_\nu)$$
$$- p^{(a)}_\gamma \eta_{\beta\mu} \eta_{\alpha\nu} + \eta_{\alpha\gamma} \eta_{\beta\mu} p^{(a)}_\nu$$
$$- p^{(b)}_\alpha \eta_{\gamma\mu} \eta_{\beta\nu} + \eta_{\beta\alpha} \eta_{\gamma\mu} p^{(b)}_\nu$$
$$- (-k^{(c)}_\beta) \eta_{\alpha\mu} \eta_{\gamma\nu} + \eta_{\gamma\beta} \eta_{\alpha\mu} (-k^{(c)}_\nu)),$$

and we use Mandlestam variables $s = (p^{(a)} + p^{(b)})^2$, $t = (k^{(c)} - p^{(a)})^2$, and $u = (k^{(G)} - p^{(a)})^2$.

In the center-of-mass frame we square the amplitude and average over initial colors and polarizations and sum over final colors and polarizations using explicit formulas for the 4−momenta and polarization vectors and tensors described in appendix B of this chapter (section 3.8). This gives the matrix element:

$$|\mathcal{A}|^2 = \frac{C_2(adj)}{dim(adj)} \frac{1}{4} \lambda^2 g_s^2 \frac{\cos^4 \theta k^2 + 6 \cos^2 \theta k^2 + 6 \cos^2 \theta m^2 + 9k^2 + 2m^2 + m^4/k^2}{(1 - \cos^2 \theta)},$$

(3.18)

where $C_2(adj)$ is the quadratic Casimir operator of the adjoint representation of the gauge group (i.e. $C_2 = N$ for $SU(N)$), $dim(adj)$ is the dimension of the adjoint representation, $k = (\sqrt{s}/2)(1 - m^2/s)$ is the graviton momentum, and θ is the angle between the initial and final momenta satisfying:

$$\cos(\theta) = \left(\frac{t - u}{s - m^2}\right).$$

(3.19)

Using:

$$\frac{d\sigma}{d\cos\theta} = \frac{1}{8\pi} \frac{k}{E_{cm}^3} |\mathcal{A}|^2,$$

(3.20)

and specializing to $SU(3)$ with $\alpha_s = g^2/(4\pi)$ gives:

$$\begin{aligned}
\frac{d\sigma}{d\cos\theta} &= \frac{3}{16} \frac{\pi \alpha_s G_N}{(1-m^2/s)(1-\cos^2\theta)} \left[(3 + \cos^2 \theta)^2 \left(1 + (\frac{m^2}{s})^4\right)\right. \\
&\quad -4 (7 + \cos^4 \theta) \frac{m^2}{s} \left(1 + (\frac{m^2}{s})^2\right) \\
&\quad \left. +6 (9 - 2\cos^2 \theta + \cos^4 \theta)(\frac{m^2}{s})^2\right].
\end{aligned}$$

(3.21)

To compute the amplitude for $q\bar{q} \to gG$ we sum the diagrams shown in figure 3.3 and use the conditions:

$$k^{(c)} \cdot \epsilon^{(c)} = k^{(G)\mu} \epsilon_{\mu\nu}^{(G)} = \eta^{\mu\nu} \epsilon_{\mu\nu}^{(G)} = 0,$$

(3.22)
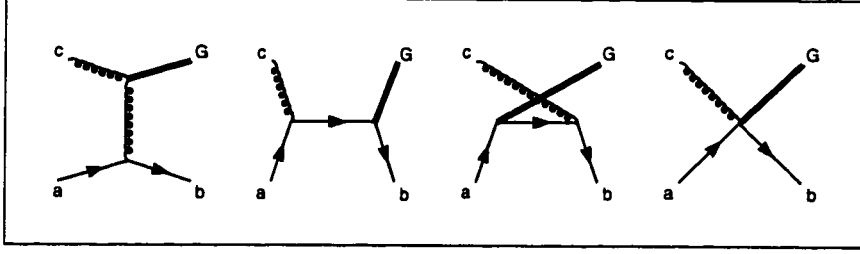
Figure 3.3: Feynman diagrams contributing to the process $q\bar{q} \to gG$.

to obtain the following expression for the amplitude for a quark with 4-momentum $p^{(a)}$ and color A and a quark with 4-momentum $p^{(b)}$ and color B to annihilate into a gluon with 4-momentum $k^{(c)}$, polarization vector $\epsilon^{(c)}$ and color c and a graviton with 4-momentum $k^{(G)}$ and polarization tensor $\epsilon^{(G)}$:

$$\mathcal{A}^c_{AB} = \lambda g t^c_{AB} u^{(a)\dagger} \left[\mathcal{A}^{(1)}_{\gamma\mu\nu} + \mathcal{A}^{(2)}_{\gamma\mu\nu} + \mathcal{A}^{(3)}_{\gamma\mu\nu} + \mathcal{A}^{(4)}_{\gamma\mu\nu} \right] u^{(a)} \epsilon^{(c)\gamma} \epsilon^{(G)\mu\nu}, \tag{3.23}$$

where we have:

$$\mathcal{A}^{(1)}_{\gamma\mu\nu} = \frac{1}{s} \Big(i q^m q^n \bar{\sigma}^k - i q^m Q^k \bar{\sigma}^n$$
$$-i\bar{\sigma} \cdot q q^n \eta^{mk} + \frac{i}{4}(q+Q) \cdot q \bar{\sigma}^n \eta^{mk} \Big)$$

$$\mathcal{A}^{(2)}_{\gamma\mu\nu} = \frac{1}{t} \Big(-\frac{i}{2} \bar{\sigma}^m p'^n \sigma \cdot (p-q) \bar{\sigma}^k \Big)$$

$$\mathcal{A}^{(3)}_{\gamma\mu\nu} = \frac{1}{u} \Big(-\frac{i}{2} \bar{\sigma}^k \sigma \cdot (p'-q) \bar{\sigma}^m p^n \Big)$$

$$\mathcal{A}^{(4)}_{\gamma\mu\nu} = +2\bar{\sigma}^m \eta^{nk}.$$

Specializing to the center-of-mass frame and using the explicit formulae for momenta and polarizations from appendix B of this chapter (section 3.8), we square the amplitude and sum over final colors and polarizations and average over and find that the helicity violating cross sections are zero, and the remaining cross sections have

$$|\mathcal{A}(q_L\bar{q}_R \rightarrow gG)|^2 = |\mathcal{A}(q_R\bar{q}_L \rightarrow gG)|^2 = |\mathcal{A}|^2 \text{ with:}$$

$$
\begin{aligned}
|\mathcal{A}|^2 = {} & \frac{\lambda^2 g^2}{16} \frac{\mathrm{tr}(\mathbf{t}^a \cdot \mathbf{t}^a)}{N_{colors}^2} \frac{s}{(1-m^2/s)^2} \left[(1 + \cos^2\theta) \left(1 + (\frac{m^2}{s})^4 \right) \right. \\
& + \left(\frac{1 - 3\cos^2\theta + 4\cos^4\theta}{1 - \cos^2\theta} \right) \frac{m^2}{s} \left(1 + (\frac{m^2}{s})^2 \right) \\
& \left. + 6\cos^2\theta(\frac{m^2}{s})^2 \right] ,
\end{aligned}
$$

$$(3.24)$$

where N_{colors} is the dimension of the quark representation of the gauge group. Using equation (3.20) and again specializing to $SU(3)$ gives:

$$
\begin{aligned}
\frac{d\sigma}{d\cos\theta} = {} & \frac{2}{9} \frac{\pi\alpha_s G_N}{(1 - m^2/s)} \left[(1 + \cos^2\theta) \left(1 + (\frac{m^2}{s})^4 \right) \right. \\
& + \left(\frac{1 - 3\cos^2\theta + 4\cos^4\theta}{1 - \cos^2\theta} \right) \frac{m^2}{s} \left(1 + (\frac{m^2}{s})^2 \right) \\
& \left. + 6\cos^2\theta(\frac{m^2}{s})^2 \right] .
\end{aligned}
$$

$$(3.25)$$

SM backgrounds may be calculated using standard four-dimensional techniques (or computed automatically using such freely-available software as MADGRAPH [40]).

3.5   Results

In this section we present the expected collider signals due to emission of gravitons into the extra dimensions appearing in [2]. The first signal considered is that of e^+e^- annihilation into an anomalous single photon recoiling against an unobserved G. This reaction could potentially be observed at the CERN e^+e^- collider LEP 2, or at a higher-energy e^+e^- collider.

The differential cross section for the reaction $e_L^- e_R^+ \rightarrow \gamma G$, considered in the center of mass system for a G of mass m can be derived from the differential cross section for the reaction $q_L\bar{q}_R \rightarrow gG$ using:

$$d\sigma_{e\bar{e}\gamma G} = \frac{9}{2}\frac{\alpha}{\alpha_s} d\sigma_{q\bar{q}gG}.$$

$$(3.26)$$

The same formula holds for $e_R^- e_L^+$; the helicity-violating cross sections are zero. These expressions must be integrated over the phase space of equation (3.11). The cross section then behaves as $\sigma \sim s^{n/2}/M^{n+2} \sim E^n/M^{n+2}$ as estimated in section 3.2. Thus, the production of anomalous single photons increases dramatically as the center-of-mass energy is raised.

In the SM, single photon events are produced in the reaction $e^+ e^- \to \gamma \nu \bar{\nu}$, which can proceed through s-channel Z^0 exchange or (for the case of ν_e) through t-channel W exchange [41]. The effect of G emission would be observable as an enhancement of the cross section for single-γ production above that of this SM source. The single-γ cross section has been measured by the LEP 2 experimental groups at $\sqrt{s} = 183$ GeV [42]. The measurements agree with the SM prediction to 6% accuracy. If we integrate our prediction for the G signal over the kinematic region studied in these experiments, we find, for the case $n = 2$, the limits $R < 0.48$ mm, $M > 1200$ GeV at 95% confidence. Limits for higher values of n are given in Table 3.1.

In Figure 3.4, we show the energy distribution of single photons recoiling against G particles for the cases $n = 2$ and $n = 6$, for the parameter values at our limit, compared to the single-photon distribution from the SM process. The peak in the SM cross section results from the process in which the γ recoils against an on-shell Z^0 which decays invisibly. Some additional advantage can be gained, then, in applying a cut which excludes this peak. For the kinematic region $20 < E_\gamma < 50$ GeV, $|\cos\theta_\gamma| < 0.95$ and $\sqrt{s} = 183$ GeV, we find the cross section for G production: $\sigma = 630/M^4, 46/M^6, 1.8/M^8$ fb. for $n = 2, 4, 6$ and M in TeV.

Higher-energy studies of $e^+ e^-$ annihilation will be done at a linear $e^+ e^-$ collider (LC). We have already noted that higher energy alone should lead to much higher sensitivity to G production. But the LC also offers another advantage, the possibility of electron beam polarization, which can be used to suppress the dominant t-channel W exchange piece of the SM background process. At $\sqrt{s} = 1$ TeV, with electron polarization $P = +0.9$ (right-handed), integrating over the kinematic region 50 GeV $< E_\gamma < 400$ GeV, $|\cos\theta_\gamma| < 0.95$, we find a SM background cross section of 82 fb and a G signal cross section of $\sigma = 20/M^4, 46/M^6, 55/M^8$ pb, for $n = 2, 4, 6$ and M in TeV. To quantify the effect of this measurement, we assume that this cross section
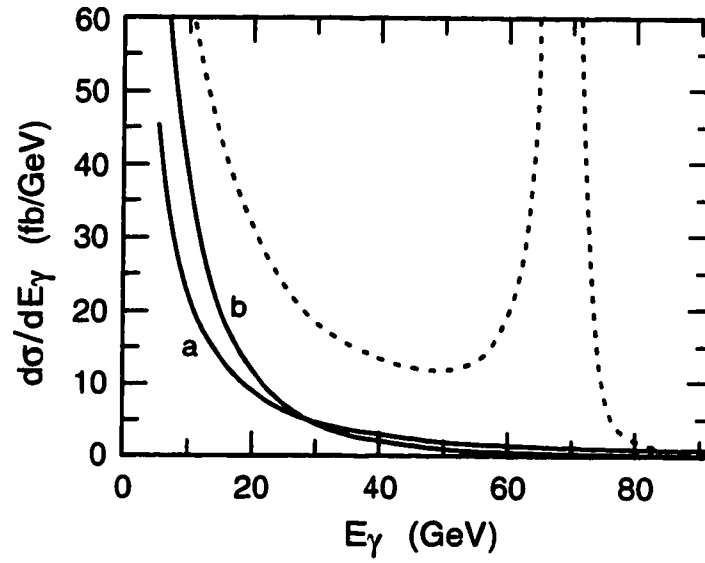
e^+e^- collisions at $\sqrt{s} = 183$ GeV with an angular cut $|\cos\theta| < 0.95$. The dotted curve is the Standard Model expectation. The solid curves show the additional cross section expected in the model of ref. 4 with (a) $n = 2$, $M = 1200$ GeV, (b) $n = 6$, $M = 520$ GeV.

Figure 3.4: Energy spectrum of single photons recoiling against higher-dimensional gravitons G.

can be measured with 5% accuracy, and that the value to be found agrees with the SM. Then the measurement would give very strong limits on R and M which are listed in Table 3.1.

The second signal considered is that of a single jet plus missing transverse energy (E_T)—which may be visible at the Fermilab Tevatron collider. The search for this reaction complements the search in e^+e^- reactions in the familiar way, with the higher energy available in hadron collisions compensating important losses in the definition of the signal.

The production of jets with large E_T recoiling against G particles can arise from the parton subprocesses $q\bar{q} \to Gg$, $qg \to qG$, $\bar{q}g \to \bar{q}G$, and $gg \to gG$. The polarization- and color-averaged cross sections for $qg \to qG$ and $\bar{q}g \to \bar{q}G$ can be obtained from the expression for $q\bar{q} \to Gg$ of equation (3.25) by re-writing it in terms of the Mandlestam variables s, t, and u and crossing $s \leftrightarrow t$. For the process $gg \to gG$, we use the polarization- and color-averaged cross section of equation (3.21).

All of these formulae must be integrated over the G mass spectrum using the measure found in equation (3.11). The rate of monojet production can then be found by integrating these cross sections with appropriate parton distributions.

The processes $q\bar{q} \to gZ^0$, $qg \to qZ^0$, followed by an invisible decay of the Z^0, give an irreducible physics background to G production. We will refer to this process as the 'SM background', and we will estimate the observability of our signal by comparing its cross section to that of this reaction. There are other important background sources from mismeasured jets and W production with forward leptons, but these backgrounds decrease sharply as the lower bound on missing E_T is increased. Unlike the case of e^+e^- reactions, the detector does not measure the imbalance in longitudinal momentum, and there is not enough kinematic information from the single observed jet to exclude the kinematic region in which the Z^0 is on-shell. On the other hand, the parton center of mass energies available at the Tevatron are higher than those of LEP 2, and we have seen that the G signal increases rapidly with energy. It is therefore reasonable to look for the monojet signal as an excess above the SM cross section for on-shell Z^0 production.

The CDF collaboration has presented a bound on monojet production based on
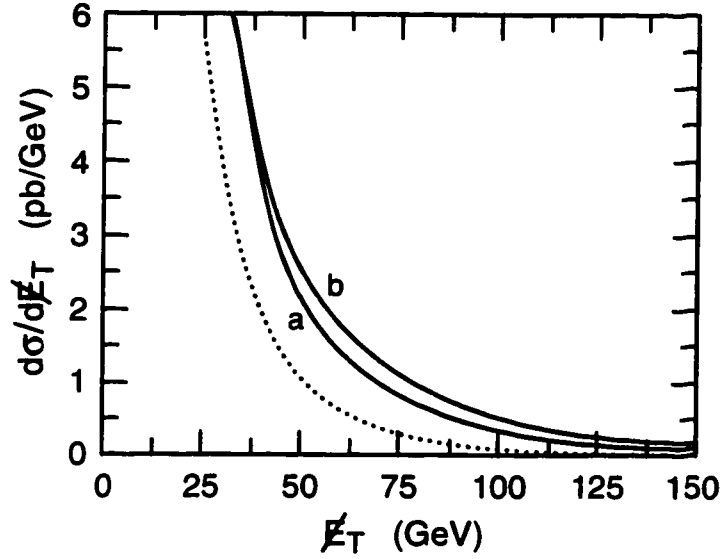
$p\bar{p}$ collisions at $\sqrt{s} = 1.8$ TeV, with a rapidity cut $|y| < 2.4$. The dotted curve is the Standard Model expectation. The solid curves show the additional cross section expected in the model of ref. 4 with (a) $n = 2$, $M = 750$ GeV, (b) $n = 6$, $M = 610$ GeV.

Figure 3.5: Spectrum of missing energy in events with one jet.

its first 4.7 pb^{-1} of data in $p\bar{p}$ collisions at $\sqrt{s} = 1.8$ TeV [43, 44]. This analysis searched for events with missing E_T greater than 30 GeV and one jet in the rapidity region $|y| < 1.2$. The result was consistent with the Z^0 background and can be represented as a limit on the number of neutrinos into which the Z^0 decays: $N_\nu < 5.0$ (95% confidence). We convert this to a limit on G production by comparing the cross sections for the G signal and the SM process, computed in the same framework. For simplicity, we carry out the calculations of both signal and background at the leading order in QCD, using the CTEQ4 lowest-order (set 3) structure functions [45]. We find a SM background cross section of 37 pb for the cuts listed above, and, for $n = 2$, a signal cross section of 20 pb/M^4. This implies a limit $R < 1.2$ mm, $M > 750$ GeV. Limits for higher values of n are given in Table 3.1. In Figure 3.5, we show the missing E_T spectrum of the signal and background processes.

It is advantageous to make a tighter cut on missing E_T to remove the backgrounds

Collider		R / M $(n = 2)$	R / M $(n = 4)$	R / M $(n = 6)$
Present:	LEP 2	4.7×10^{-2} / 1200	1.9×10^{-9} / 730	6.9×10^{-12} / 520
	Tevatron	11.0×10^{-2} / 750	2.4×10^{-9} / 610	5.8×10^{-12} / 610
Future:	Tevatron	3.9×10^{-2} / 1300	1.4×10^{-9} / 900	4.0×10^{-12} / 810
	LC	1.2×10^{-3} / 7700	1.2×10^{-10} / 4500	6.5×10^{-13} / 3100
	LHC	3.4×10^{-3} / 4500	1.9×10^{-10} / 3400	6.1×10^{-13} / 3300

Table 3.1: Current and future sensitivities to large extra dimensions, expressed as 95% confidence limits on the size of extra dimensions R (in cm) and the effective Planck scale M (in GeV). The assumptions of each analysis are explained in the text.

from mismeasured jets which were a problem for the CDF analysis [43]. Integrating the signal and background rates over the region with missing $E_T > 60$ GeV and jet rapidity $|y| < 2.4$, we find a SM background cross section for Z production of 10 pb, and signal cross sections in the ratios $S/B = 0.85/M^4, 0.15/M^6, 0.052/M^8$, for $n = 2, 4, 6$ and M in TeV. Assuming that this measurement can be performed with 20% accuracy, and that the value to be found agrees with the SM, we find the potential limits on R and M listed in the third line of Table 3.1.

Hadron-hadron collisions will be studied at higher energy at the CERN LHC. We find that both the signal and the SM background processes are dominated by $q\bar{q}$ and qg collisions. Repeating the analysis at the LHC energy of 14 TeV using the kinematic cuts $E_T > 200$ GeV, $|y| < 5$, we find a SM background cross section of 11 pb and signal cross sections in the ratios $S/B = 110/M^4, 420/M^6, 3600/M^8$, for $n = 2, 4, 6$ and M in TeV. With the same assumptions as before, we find the potential limits listed in the last line of Table 3.1. It is important to note that, in the case $n = 6$, the dominant parton-parton center of mass energies are comparable to the quoted limit on M, so the effective coupling of equation (3.7) might not be appropriate for this case.

3.6   Conclusions

In this chapter, we have shown that high-energy collider searches for events with missing energy and transverse momentum provide a relevant, model-independent test of theories with large extra space dimensions. Current high-energy experiments at e^+e^- and $p\bar{p}$ colliders already place strong direct constraints on these theories. Higher-energy experiments may place much stronger constraints. Or, more optimistically, they may allow us to observe an excess of missing-energy events above the SM expectation, providing direct evidence for this remarkable extension of our conception of the universe.

3.7   Appendix A:
Fermion Couplings

Fermion couplings to the gravitational field derive from the kinetic term:

$$\mathcal{L} \sim i\psi^\dagger e^\mu_a \sigma^a (\partial_\mu + \frac{1}{2}\omega^{ab}_\mu \sigma_{ab})\psi, \tag{3.27}$$

and thus require tetrads e^a_μ and spin connections ω^{ab}_μ consistent with the induced metric on the four-dimensional membrane. The tetrad must satisfy:

$$e^a_\mu e^b_\nu \eta_{ab} = g_{\mu\nu}, \tag{3.28}$$

which may be related to the graviton wave-function $h_{\mu\nu}$ by a perturbative solution in the gravitational coupling λ. For Euclidean signatures the consistency condition of equation (3.28) is the matrix equation $\mathbf{e}^T \cdot \mathbf{e} = \mathbf{g}$, and with the gauge choice $e^b_a = e^a_b$ (i.e. $\mathbf{e}^T = \mathbf{e}$), this consistency condition becomes $\mathbf{e} \cdot \mathbf{e} = \mathbf{g}$ and has the following solution to arbitrary order in λ:

$$\mathbf{e} \cdot \mathbf{e} = \mathbf{g} = 1 + \lambda\mathbf{h}$$
$$\mathbf{e} = \sqrt{1 + \lambda\mathbf{h}} \equiv 1 + \frac{\lambda}{2}\mathbf{h} - \frac{\lambda^2}{8}\mathbf{h}\cdot\mathbf{h} + ... \tag{3.29}$$

where the matrix square root is defined by its Taylor expansion. To first order in λ, we may simply use:

$$e_{\alpha\rho} = \eta_{\alpha\rho} + \frac{1}{2}\lambda h_{\alpha\rho}. \tag{3.30}$$

The spin connection may be derived from the tetrad:

$$\begin{aligned}
\omega_\mu^{ab} &= \frac{1}{2}g^{\rho\nu}e_\rho^{[a}\partial_{[\mu}e_{\nu]}^{b]} + \frac{1}{4}g^{\rho\nu}g^{\tau\sigma}e_\rho^{[a}e_\tau^{b]}\partial_{[\sigma}e_{\nu]}^a e_\mu^d\eta_{ad} \\
&= -\frac{\lambda}{2}\partial^{[a}h_\mu^{b]} + O(\lambda^2).
\end{aligned} \tag{3.31}$$

3.8 Appendix B:

Center-of-mass Momenta and Polarizations

For both $gg \to gG$ and $q\bar{q} \to Gg$ we use the geometry displayed in figure 3.6 and the following expressions for the momenta and final-state particle polarizations:

$$p^{(a)} = \frac{\sqrt{s}}{2}\begin{pmatrix} 1 \\ \sin(\theta) \\ 0 \\ \cos(\theta) \end{pmatrix}, \quad p^{(b)} = \frac{\sqrt{s}}{2}\begin{pmatrix} 1 \\ -\sin(\theta) \\ 0 \\ -\cos(\theta) \end{pmatrix},$$

$$k^{(c)} = k\begin{pmatrix} 1 \\ 0 \\ 0 \\ -1 \end{pmatrix}, \quad \epsilon_\pm^{(c)} = \frac{1}{\sqrt{2}}\begin{pmatrix} 0 \\ 1 \\ \mp i \\ 0 \end{pmatrix},$$

$$k^{(G)} = k\begin{pmatrix} \sqrt{\frac{m^2}{k^2}+1} \\ 0 \\ 0 \\ 1 \end{pmatrix}, \quad \epsilon_{\pm 2}^{(G)} = \frac{1}{2}\begin{pmatrix} 0 & 0 & 0 & 0 \\ 0 & 1 & \pm i & 0 \\ 0 & \pm i & -1 & 0 \\ 0 & 0 & 0 & 0 \end{pmatrix},$$

$$\epsilon_{\pm 1}^{(G)} = \frac{k}{2m}\begin{pmatrix} 0 & 1 & \pm i & 0 \\ 1 & 0 & 0 & \sqrt{1+m^2/k^2} \\ \pm i & 0 & 0 & \pm i\sqrt{1+m^2/k^2} \\ 0 & \sqrt{1+m^2/k^2} & \pm i\sqrt{1+m^2/k^2} & 0 \end{pmatrix},$$
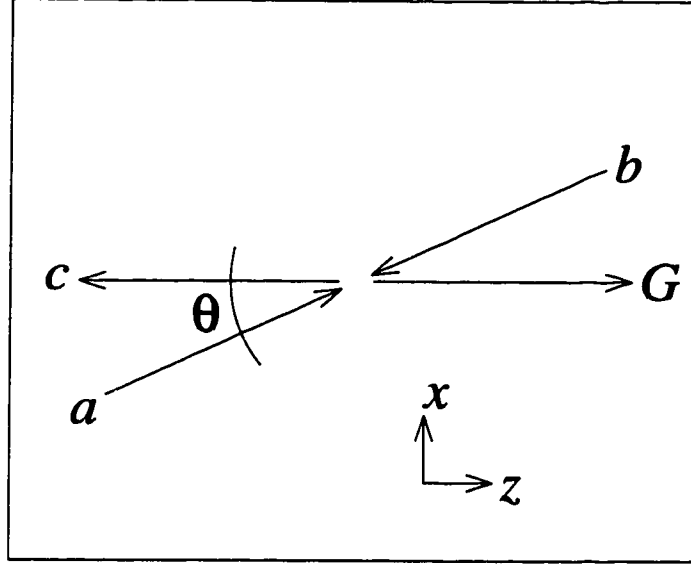
Figure 3.6: Center-of-mass reaction geometry.

$$
\epsilon_0^{(G)} = \tfrac{1}{\sqrt{6}}
\begin{pmatrix}
-2k^2/m^2 & 0 & 0 & -2k^2/m^2\sqrt{1+m^2/k^2} \\
0 & 1 & 0 & 0 \\
0 & 0 & 1 & 0 \\
-2k^2/m^2\sqrt{1+m^2/k^2} & 0 & 0 & -2(1+k^2/m^2)
\end{pmatrix}.
\tag{3.32}
$$

For $gg \to gG$ we use initial-state particle polarizations:

$$
\epsilon_\pm^{(a)} = \tfrac{1}{\sqrt{2}}
\begin{pmatrix}
0 \\
\cos(\theta) \\
\pm i \\
-\sin(\theta)
\end{pmatrix}, \qquad
\epsilon_\pm^{(b)} = \tfrac{1}{\sqrt{2}}
\begin{pmatrix}
0 \\
\cos(\theta) \\
\mp i \\
-\sin(\theta)
\end{pmatrix},
\tag{3.33}
$$

and for $q\bar{q} \to Gg$ we use initial-state particle polarizations:

$$
u^{(a)}_{h=\frac{+1}{2}} = (\sqrt{s})^{1/2}
\begin{pmatrix}
\cos(\theta/2) \\
\sin(\theta/2)
\end{pmatrix} \qquad
u^{(a)}_{h=-\frac{1}{2}} = (\sqrt{s})^{1/2}
\begin{pmatrix}
-\sin(\theta/2) \\
\cos(\theta/2)
\end{pmatrix},
$$

$$
u^{(b)}_{h=\frac{+1}{2}} = (\sqrt{s})^{1/2}
\begin{pmatrix}
-\cos(\theta/2) \\
-\sin(\theta/2)
\end{pmatrix}, \qquad
u^{(b)}_{h=-\frac{1}{2}} = (\sqrt{s})^{1/2}
\begin{pmatrix}
-\sin(\theta/2) \\
\cos(\theta/2)
\end{pmatrix}.
\tag{3.34}
$$

Chapter 4

Yukawa Hierarchies From Displaced Fermions

Here we explore Arkani-Hamed and Schmaltz's mechanism for generating hierarchies among Yukawa couplings through the relative displacement of the locations of the standard model fields within a four-dimensional membrane in a higher-dimensional space. We find only one configuration of displacements consistent with experiment, with a prediction for the strange quark mass $m_s^{\overline{MS}}(2\ GeV) \approx (1.19) \times (V_{ub}V_{cb}/V_{us})^{1/2} \times m_b^{\overline{MS}}(m_b) \approx 120\ MeV$.

4.1 Introduction

The parameters of the standard model contain a mystery: why do the Yukawa couplings vary over so many orders of magnitude? The up quark Yukawa coupling is of order unity, which we would naïvely expect, but the other couplings are strewn randomly over several orders of magnitude below this. Why are most matter particles so light?

Traditional explanations of this Yukawa hierarchy invoke new symmetries, but in [47] Arkani-Hamed and Schmaltz suggested an explanation which operates in the absence of any special symmetries. They suggest that the hierarchies present in the Yukawa couplings of the standard model can be explained as a result of the slight

displacement of the standard model field wavefunctions inside a four-dimensional domain wall in a higher-dimensional space. The effective four-dimensional Yukawa is a product of the fundamental higher-dimensional Yukawa coupling and the overlap of the field wavefunctions. If the wavefunctions are highly peaked, a small relative shift between wavefunctions leads to a large suppression of the effective Yukawa through the smallness of the overlap of the wavefunctions. Even with a single $O(1)$ higher-dimensional Yukawa coupling, one could produce Yukawa hierarchies through the relative displacements of the wavefunction peaks.

They provide a natural, field-theoretic mechanism for producing such displacements, and demonstrate how it can lead to the appearance of a small Yukawa coupling, but their discussion is very general, which raises the question of whether a realistic model using their mechanism could actually be constructed, or whether their are hidden constraints and relations among the masses and mixing angles of the standard model that preclude their generation from a set of displaced wavefunctions.

In this chapter, we seek to address this question. We find that while it is easy to arrange two- (or higher) dimensional arrays of wavefunctions which reproduce the parameters of the standard model, it is difficult (but not impossible!) to do so in a minimal one-dimensional version; we find essentially one possible configuration of wavefunctions, and out of the constraints on this configuration we find a definite prediction, which may be confirmed or falsified by more accurate determinations of the strange quark mass.

In section 4.2, we summarize the mechanism of [47], and in section 4.3 we summarize the outline of a model suggested in that paper. In section 4.4 we demonstrate the mechanism on the simple case of the lepton sector, and in section 4.5 we outline the challenges present when trying to model the quark sector. In section 4.6 we describe our efforts to find a set of locations for the quark wavefunctions, and in section 4.7 we analyze the (essentially) unique set, which leads to the prediction for the strange quark mass $m_s \approx (1.19) \times m_b (V_{ub} V_{cb} / V_{us})^{1/2} \approx 120 \ MeV$. Section 4.8 presents a complete landscape of wavefunctions, with the separation of the quark and lepton wavefunctions chosen to safely suppress proton decay, and we briefly conclude in section 4.9. The first appendix to this chapter (section 4.10) contains a derivation of the

form of the zero mode for a minimal five-dimensional spinor coupled to a scalar with a domain wall profile expectation value. The second appendix to this chapter (section 4.11) contains the experimentally allowed masses and mixings we used, as well as the renormalization multipliers used to evaluate those parameters at a common scale.

4.2 Producing Hierarchies With Exponentially Small Overlaps

In this section, we summarize the mechanism of [47] for producing hierarchies between mass matrix elements. We start by considering a theory in which the standard model fermions are trapped in a four-dimensional membrane in a five-dimensional space. Although non-perturbative effects in string/M theory can be used to achieve such localizations, one can also study models in which the localization occurs in the context of an effective field theory.

One concrete field-theory method of achieving such a localization is to couple a massless five-dimensional fermion Ψ to a five-dimensional scalar field Φ through a Yukawa coupling term $\sim \int d^5x \Phi \bar{\Psi} \Psi$ in the Lagrangian, and then to include an effective potential for Φ with two or more isolated vacua (such as a Φ^4 potential), so that it attains a position-dependent vacuum expectation value with a domain-wall profile in the extra dimension, interpolating between regions with different choices of vacuum (see figure 4.1).

The fermion then acquires a zero-energy state localized near the zero-crossing of Φ. Heuristically, one may think of the Yukawa coupling to the position-dependent scalar expectation value as giving the fermion a position-dependent mass which greatly suppresses field fluctuations far from the domain wall at $x_5 = 0$ while leaving fluctuations at the origin massless. Although a single minimal spinor in five-dimensional space decomposes into a left-right mirror pair of chiral fermions in four-dimensional language, only one chirality zero-energy state is trapped on the wall.

In the first appendix of this chapter (section 4.10) we derive the zero mode solution in the approximation in which the scalar field profile is a linear function of the extra
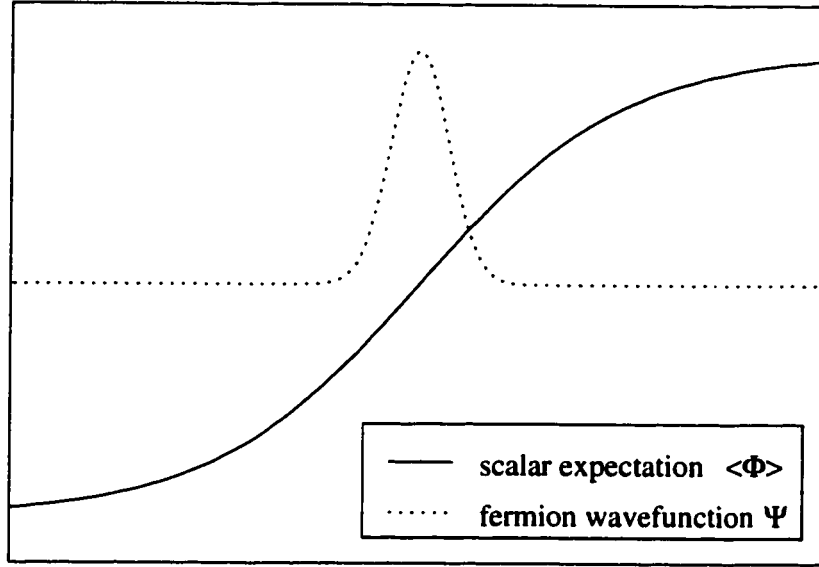
Figure 4.1: A chiral fermion trapped on a domain wall.

dimension $\Phi = 2\mu^2 x_5$ (which is valid for points close to the center of the domain wall $\mu x_5 \ll L$) and find that zero mode solutions for the fermions have Gaussian profiles in the extra dimension centered on the zero of $\Phi(x_5)$:

$$\Psi(x) = A \, e^{-\mu^2 x_5^2} \times \psi(x_0, x_1, x_2, x_3), \tag{4.1}$$

where ψ is a canonically normalized massless left-handed four-dimensional fermion field, $A = \mu^{1/2}(\pi/2)^{-1/4}$ is a normalization constant, and μ is related to the slope of the scalar field profile by $\mu^2 = \partial_5\langle\Phi\rangle/2$. Higher modes, which come in mirror pairs, have minimum energy $\approx \mu$.

In [47], it was pointed out that adding a five-dimensional fermion mass term $\int d^5 x M\overline{\Psi}\Psi$ to the above system acts like an effective shift of the scalar field $\Phi \to \Phi + M$ as far as the fermion is concerned, which (in the approximation in which the scalar field profile is linear) leads to an effective shift of the location where the scalar has a zero expectation value, i.e., a shift in the effective location of the domain wall as seen by the fermion (see figure 4.2) so that it ends up localized around $\ell_5 = -M/2\mu^2$. If different fermions have different masses M_i, they each end up localized
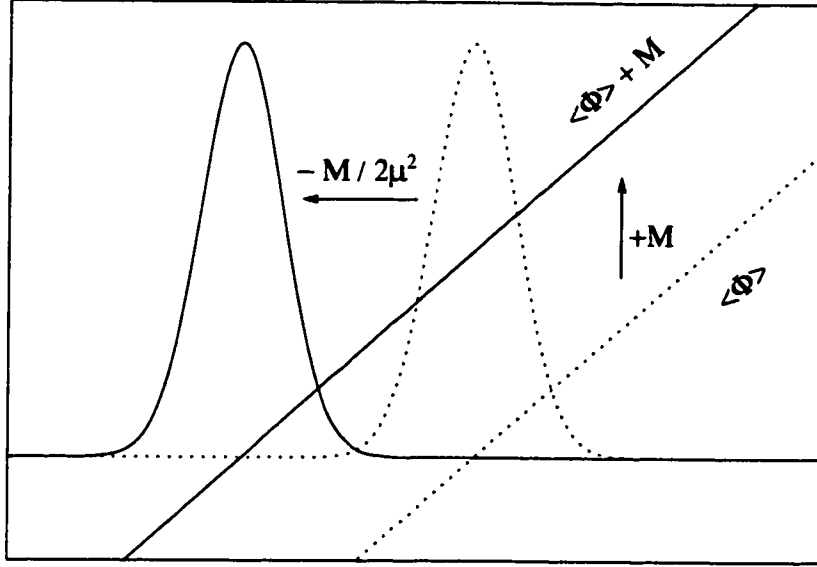
Figure 4.2: A mass term shifts the location of the domain wall.

around different locations $\ell_{(i)5} = -M_i/2\mu^2$, each fermion being centered on a different "effective" zero of the same scalar field.

Assuming a generic five-dimensional Yukawa coupling between two fermions and a Higgs scalar field H (assumed for simplicity to have a constant profile in the extra dimension) leads, upon substitution of the zero mode solution from equation (4.1) and integration over the extra dimension, to a four dimensional coupling modulated by the mutual overlap of the fermion wavefunctions:

$$\mathcal{L}_{Yukawa} = \int d^5x \; \kappa H \overline{\Psi}_1 \Psi_2 \tag{4.2}$$

$$= \int d^5x \; \kappa H \left(A \; e^{-\mu^2(x_5-\ell_1)^2} \psi_1 \right) \left(A \; e^{-\mu^2(x_5-\ell_2)^2} \psi_2 \right) \tag{4.3}$$

$$= \int d^4x \left(\int dx_5 \; \kappa A \; e^{-\mu^2(x_5-\ell_1)^2} A \; e^{-\mu^2(x_5-\ell_2)^2} \right) H \psi_1 \psi_2 \tag{4.4}$$

$$= \int d^4x (e^{-\frac{1}{2}\mu^2(\ell_1-\ell_2)^2} \kappa) H \psi_1 \psi_2 \tag{4.5}$$

$$= \int d^4x \lambda H \psi_1 \psi_2, \tag{4.6}$$

where the effective four-dimensional Yukawa coupling:

$$\lambda = e^{-\frac{1}{2}\mu^2(\ell_1-\ell_2)^2}\kappa, \tag{4.7}$$

depends on the mutual overlap of the zero modes of the fermions through the relative displacement of their peaks $|\ell_1 - \ell_2|$. If the fermions are more than a few Gaussian widths μ^{-1} from each other then an order-one coefficient for the five-dimensional Yukawa coupling κ results in an exponentially small four-dimensional Yukawa coupling λ. Setting the Higgs field to its expectation value and generalizing to many generations gives a mass matrix element:

$$
\begin{aligned}
m_{ij} &= (\langle H \rangle\, \kappa)\; e^{-\frac{1}{2}\mu^2(\ell_i-\ell_j)^2} \\
&= \rho\, e^{-\frac{1}{2}\mu^2(\ell_i-\ell_j)^2},
\end{aligned}
\tag{4.8}
$$

where $\rho \equiv \langle H \rangle\, \kappa$. In this paper we seek to obtain the hierarchical pattern of masses and mixings in the standard model as a result of a particular configuration of wavefunction locations with relative separations of a few Gaussian widths μ^{-1}.

It is useful to invert equation (4.8) to find the relative displacements associated with a mass matrix:

$$|\ell_i - \ell_j| = \mu^{-1}\sqrt{-2\,\log(m_{ij}/\rho)} \equiv p(m_{ij}). \tag{4.9}$$

To produce a particular mass matrix m_{ij}, we need to find a set of wavefunction locations which have relative displacements $|\ell_i - \ell_j|$ related to the mass matrix by the above formula. The function $\mu^{-1}\sqrt{-2\,\log(m_{ij}/\rho)}$ appears often in expressions to follow; we refer to this function as $p(m_{ij})$.

4.3 The Model

We now summarize the model outlined in [47]. By the standard model gauge symmetry, all fields in a given gauge multiplet are assumed to have the same effective five dimensional fermion mass M_i and thus are assumed to have wavefunctions peaked at

the same location in the extra dimension. This means that there are fifteen wavefunction locations q_i, u_i, d_i, l_i and e_i for the left-handed standard model fields Q_i, U_i^c, D_i^c, L_i and E_i^c (with $i = 1, 2, 3$). The fermions are all taken to have equal couplings to the domain wall scalar Φ (meaning their Gaussian wavefunctions all have equal widths), and so as not to add extra complication, we take the Higgs field H to have an expectation value which is constant throughout the domain wall, and we take the effective five dimensional Yukawa couplings between the fermions and the Higgs to have a single magnitude. Although these restrictions could be relaxed, the structure already present proves sufficient to generate the standard model masses and mixings. We defer a discussion of the CP violating complex phase of the CKM matrix to later work, and for the present time study only real Yukawa matrices.

The analysis of Arkani-Hamed and Schmaltz constrains the scales present in the model. For the description to make sense, we need the wall thickness L to be larger than the Gaussian width μ^{-1}, which in turn should be larger than the length scale of the ultraviolet cutoff $1/M_*$. For the four dimensional effective top Yukawa coupling λ_t to be perturbative at M_* we must further constrain $N\lambda_t^2/16\pi^2 < 1$ where $N = (M_*L)/2\pi$ is the number of Kaluza-Klein modes below the cutoff. If a field theory description is to apply throughout the wall, we must have $\Phi(L/2) \sim \mu^2 L/2 < M_*$. And finally, the width of the wall should not be much larger than a TeV^{-1} for consistency with the conventional physics observed at colliders. To summarize:

$$L^{-1} \;\; < \;\; \mu < M_* \tag{4.10}$$

$$M_*/L^{-1} \;\; < \;\; 32\pi^3/\lambda_t^2 \approx 1000 \tag{4.11}$$

$$\mu/L^{-1} \;\; < \;\; \sqrt{2M_*/L^{-1}} \approx 44 \tag{4.12}$$

$$L^{-1} \;\; > \;\; O(1) \text{ TeV}. \tag{4.13}$$

In equation (4.8) the mass matrix element is bounded from above by ρ, with the maximal value achieved when the fermion wavefunctions are localized around the same point. This means that to generate the top mass from a single matrix element the condition $\rho > m_t$ is required. On the other hand, naturalness and perturbativity of couplings lead us to want ρ as small as possible. For concreteness, we choose

ρ to be 1.5 m_t. Our model works for any $\rho \geq m_t$, with larger ρ values requiring greater suppressions from the overlaps, and thus requiring larger separations between wavefunctions. The mass prediction of equation (4.43) is independent of ρ, since the wavefunction positions are always chosen to reproduce the same mass matrices.

Before trying to reproduce the masses of the standard model, we first run the masses of the standard model to a common scale m_t using the scaling factors found in the appendix (the running of the CKM elements to that scale is small compared to the experimental uncertainty in their magnitudes).

4.4 Lepton sector of the model

We begin our efforts to reproduce the standard model masses and mixings by finding a set of wavefunction positions for the L_i and E_i^c fields which reproduce the observed charged lepton masses. This is easy, since we are only trying to fit three parameters and we may adjust five parameters (six locations, minus one freedom to shift the locations by an overall displacement since only relative locations matter in equation (4.8)). Assuming a simple diagonal texture for the lepton mass matrix:

$$\mathbf{m_e} = \begin{pmatrix} m_e & 0 & 0 \\ 0 & m_\mu & 0 \\ 0 & 0 & m_\tau \end{pmatrix}, \tag{4.14}$$

leads, using equation (4.9) to a matrix of relative distances:

$$|l_i - e_j| = \mu^{-1} \begin{pmatrix} 5.1275 & (far) & (far) \\ (far) & 3.9475 & (far) \\ (far) & (far) & 3.1498 \end{pmatrix}. \tag{4.15}$$

We have three constraints on the locations, with the only other constraints being that the relative displacements indicated by (far) be great enough to lead to negligible off-diagonal matrix elements. In fact, it turns out that little care is necessary to insure that the off-diagonal elements are negligible; one need only insure that, for a given L field, the closest E^c field is roughly one width closer than the second-closest E^c field.

It proves to be a general property of this model, due to the exponential in equation (4.8), that if one wavefunction is near two others and the two others are not the same distance away then the overlap with the farther one will often be negligible compared to the overlap with the closer one. In other words, it is easy to generate elements of the Yukawa matrix that are effectively zero.

One possible set of locations for the lepton fields is:

$$l_i = \mu^{-1} \begin{pmatrix} 11.075 \\ 1.0 \\ 0.0 \end{pmatrix} = \begin{pmatrix} e_2 + \mu^{-1} + p(m_\mu) \\ l_3 + \mu^{-1} \\ 0 \end{pmatrix} \tag{4.16}$$

$$e_i = \mu^{-1} \begin{pmatrix} 5.9475 \\ 4.9475 \\ -3.1498 \end{pmatrix} = \begin{pmatrix} l_1 - p(m_e) \\ l_2 + p(m_\mu) \\ l_3 - p(m_\tau) \end{pmatrix} .. \tag{4.17}$$

This configuration is depicted graphically in figure 4.3. This is by no means the only set of wavefunction locations that reproduce the e, μ, and τ masses. For instance, the mass spectrum is essentially unchanged if one moves the L_i further apart while keeping each E_i^c wavefunction the same distance from its partner L_i (i.e. replacing the μ^{-1} with a larger distance in equations (4.16) and (4.17). Also, one can consider textures differing from that of equation (4.14)—since lepton mixing angles are unobservable, all that is necessary is that the eigenvalues of the mass matrix equal the lepton masses. Different textures would lead to different sets of wavefunction locations.

4.5   Quark sector of the model

We now outline the challenges present when trying to model the quark sector. It is more difficult than the lepton sector because one has to fit nine observables (six masses and three mixing angles) by adjusting eight parameters (the nine locations of the Q_i, U_i^c, and D_i^c, minus one freedom to shift the locations by an overall displacement).

In fact, equation (4.8) determines the mass matrices $\mathbf{m_u}$ and $\mathbf{m_d}$. To obtain the physical masses and CKM elements from the mass matrices we must perform unitary redefinitions of the $Q_{(I=+1/2)i}$, $Q_{(I=-1/2)i}$, U_i^c and D_i^c fields to a basis where the mass
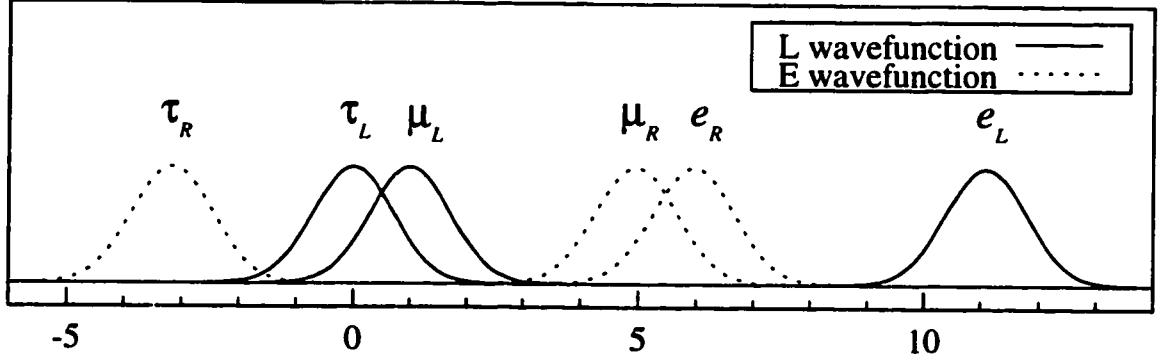
In this and following diagrams, the fields, when possible, have been labeled by their more common names, such as $E_1 = e_R$, $E_2 = \mu_R$, $E_3 = \tau_R$, etc.

Figure 4.3: The locations of the lepton wavefunctions.

matrices are diagonal. The masses can be read off the diagonal entries, and the CKM matrix appears in the weak interaction terms as a result of the mismatch between the redefinitions of the isospin-up and isospin-down components of the quark doublets.

A useful method of computing the parameters is to calculate[48]:

$$\mathbf{m_u m_u^\dagger} = \mathbf{U_u} \begin{pmatrix} m_u^2 & 0 & 0 \\ 0 & m_c^2 & 0 \\ 0 & 0 & m_t^2 \end{pmatrix} \mathbf{U_u^\dagger} \tag{4.18}$$

$$\mathbf{m_d m_d^\dagger} = \mathbf{U_d} \begin{pmatrix} m_d^2 & 0 & 0 \\ 0 & m_s^2 & 0 \\ 0 & 0 & m_b^2 \end{pmatrix} \mathbf{U_d^\dagger} \tag{4.19}$$

$$\mathbf{V_{CKM}} = \mathbf{U_u^\dagger U_d}. \tag{4.20}$$

The eigenvalues of the hermitian squares of the up(down) mass matrices give the squares of the masses of the up(down) type quarks, and the products of the eigenvectors of the hermitian square of the up mass matrix with the eigenvectors of the hermitian square of the down mass matrix give the CKM matrix elements. Ignoring the CP violating complex phase, it is sufficient to match the magnitudes of the three components of the CKM matrix above the diagonal to match the entire matrix.

However, we seek to do more than simply reproduce the standard model masses and mixing angles—we seek to reproduce the hierarchies present in a natural way, as a result of the exponential in equation (4.8). This excludes certain mass matrix textures from consideration.

For example, consider the mass matrices:

$$\begin{pmatrix} 0 & 0 \\ 0 & 1 \end{pmatrix} \quad \text{and} \quad \begin{pmatrix} .5 & .5 \\ .5 & .5 \end{pmatrix}. \tag{4.21}$$

Both yield a spectrum with a hierarchy (in fact, they each yield a spectrum containing one massless and one massive particle) but in the first matrix the hierarchy is a result of the hierarchy between the last element and all the other elements, which equation (4.8) easily produces, while in the second matrix the hierarchy is a result of a delicate cancellation between all the matrix elements, which would be exponentially fine-tuned if these elements came from equation (4.8). Although these fine tunings could possibly be explained by adding further symmetries, our philosophy is to seek a set of generic-looking positions which lead to small masses and mixings as a result of small numbers coming from the exponential in (4.8). We only allow small numbers to come from the product of small numbers, but not from a cancellation or sum. One might be tempted to allow cancellations or sums from numbers which are of the same order-of-magnitude as the quantity they cancel or sum to produce, since it does not seem like fine-tuning to have $O(\epsilon^n) \pm O(\epsilon^n) = O(\epsilon^n)$, but we avoid doing this here because in this model it would usually involve an unexplained coincidence—generically any two elements of the mass matrix resulting from equation (4.8) have vastly different orders of magnitude and it takes a strange coincidence or a fine tuning for two elements to have an $O(1)$ ratio. An exception to this is the third generation: the masses of the top and bottom approach the upper-bound scale ρ, and as we approach this scale such coincidences become less fine-tuned[1], so we allow models which produce a mass parameter $\sim m_t$ or $\sim m_b$ through the sum or difference of two terms of roughly that order of magnitude. We first consider the case where m_t comes from a single mass

---

[1]The fine tuning $\partial m_{ij}/\partial \ell_j \to 0$ as $|\ell_i - \ell_j| \to 0$, which happens when $m_{ij} \to \rho$. For $|\ell_i - \ell_j|$ larger than a few widths μ^{-1}, that is, for m_{ij} below the mass scale of the third generation, $\partial m_{ij}/\partial \ell_j$ grows rapidly.

matrix element and m_b also comes from a (different) single matrix element (we will later need to relax the constraint on m_b).

A simple mass matrix texture appropriate to our philosophy is:

$$\mathbf{m_u} = \begin{pmatrix} m_u & 0 & 0 \\ 0 & m_c & 0 \\ 0 & 0 & m_t \end{pmatrix} \tag{4.22}$$

$$\mathbf{m_d} = \begin{pmatrix} m_d & m_s V_{us} & m_b V_{ub} \\ 0 & m_s & m_b V_{cb} \\ 0 & 0 & m_b \end{pmatrix} \approx \mathbf{V_{CKM}} \cdot \begin{pmatrix} m_d & 0 & 0 \\ 0 & m_s & 0 \\ 0 & 0 & m_b \end{pmatrix}, \tag{4.23}$$

in which each small mass and mixing arises directly from the exponential suppression of equation (4.8).

We now try to construct these matrices from the model. Translating the matrices from equations (4.22) and (4.23) into a matrix of constrained relative distances using equation (4.9) gives:

$$|q_i - u_j| = \mu^{-1} \begin{pmatrix} 4.8701 & (far) & (far) \\ (far) & 3.4840 & (far) \\ (far) & (far) & .90052 \end{pmatrix} \tag{4.24}$$

$$|q_i - d_j| = \mu^{-1} \begin{pmatrix} 4.7416 & 4.4278 & 4.5319 \\ (far) & 4.0715 & 3.9378 \\ (far) & (far) & 3.0029 \end{pmatrix}. \tag{4.25}$$

These constraints can easily be satisfied in two-dimensional extensions of the current model involving string defects in place of domain walls (see figure 4.4). Unfortunately, the configuration cannot be collapsed down to one dimension without bringing some wavefunctions too close to preserve the smallness of the "zero" elements of the texture.

A similar texture can be found by taking the down mass matrix diagonal and using:

$$\mathbf{m_u} = \begin{pmatrix} m_u & m_c V_{us} & m_t(1 - V_{ub}) \\ 0 & m_c & m_t V_{cb} \\ 0 & 0 & m_t \end{pmatrix} \approx \mathbf{V_{CKM}^\dagger} \cdot \begin{pmatrix} m_u & 0 & 0 \\ 0 & m_c & 0 \\ 0 & 0 & m_t \end{pmatrix}, \tag{4.26}$$
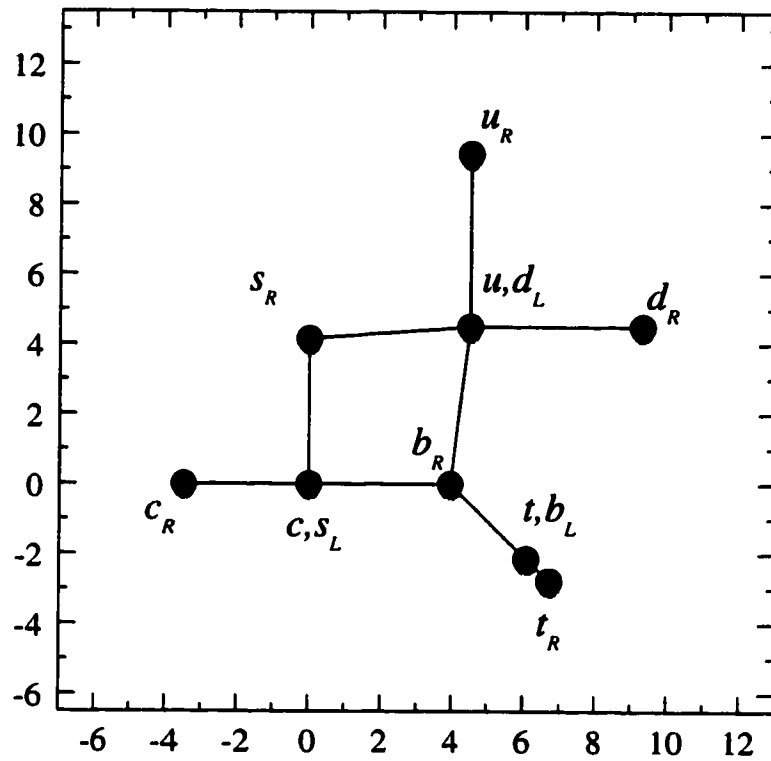
(The lines represent constrained distances between wavefunction locations.)

Figure 4.4: A possible set of locations for quark wavefunctions in a model with two extra dimensions.

and, at the same level of approximation, one can use textures where two of the V_{CKM} elements come from one mass matrix and one comes from the other. The textures can be further extended by allowing the small masses to result from products of two small mass matrix entries by generalizing the observation that the 2×2 mass matrix:

$$\begin{pmatrix} 0 & b \\ c & D \end{pmatrix},$$
(4.27)

with $b, c \ll D$ has masses D and bc/D. For instance, the mass matrix:

$$\mathbf{m_d} = \begin{pmatrix} 0 & m_s V_{us} & m_b V_{ub} \\ m_d/V_{us} & m_s & m_b V_{cb} \\ 0 & 0 & m_b \end{pmatrix},$$
(4.28)

leads to a down quark mass m_d.

4.6 Searching Parameter Space

In this section we describe our efforts to find a set of locations for the quark wavefunctions. The textures described in section 4.5 (where each mixing parameter comes from a nonzero above-diagonal element in either the up mass matrix or the down mass matrix, and the masses come from either a diagonal element or a product of a below-diagonal element and an above-diagonal mixing term) were searched analytically with no success. The closest match allowed one to fit all the masses and two of the mixings by hand, with all the "zero" elements of the texture being of negligible magnitude. Fitting these parameters determined all the wavefunction positions, and thus predicted the remaining mixing (parameterized by V_{ub}) which was found to be many orders of magnitude too small. We then resorted to numerical methods, and also relaxed our assumptions to allow for m_t to result from the contributions of two or more elements of roughly equal magnitude (and later extended this relaxation to m_b).

We implemented a brute-force scan over the parameter space, which yielded a solution with two mass matrix elements of magnitude m_b described in section 4.7

below.

4.7 Analysis of Solution

We now describe the configuration of quark wavefunction locations which was found to produce agreement with the observed masses and mixings of the standard model. The configuration:

$$q_i = \mu^{-1} \begin{pmatrix} -7.6057 \\ 6.9522 \\ 0.0 \end{pmatrix} \approx \begin{pmatrix} d_2 - p(m_s V_{us}/\cos(\theta)) \\ d_3 + p(m_b V_{cb}/\cos(\theta)) \\ 0 \end{pmatrix} \quad (4.29)$$

$$u_i = \mu^{-1} \begin{pmatrix} -2.7357 \\ 10.4362 \\ 0.9012 \end{pmatrix} \approx \begin{pmatrix} q_1 + p(m_u) \\ q_2 + p(m_c) \\ q_3 + p(m_t) \end{pmatrix} \quad (4.30)$$

$$d_i = \mu^{-1} \begin{pmatrix} 11.3682 \\ -3.2250 \\ 3.0511 \end{pmatrix} \approx \begin{pmatrix} q_2 + p(m_d/V_{us}) \\ q_3 - p(m_d\sin(\theta)) \\ q_3 + p(m_d\cos(\theta)) \end{pmatrix}, \quad (4.31)$$

was found to produce mass matrices:[2]

$$\mathbf{m_u} = \begin{pmatrix} 1.7630 & 5.1637 \times 10^{-66} & 4.8087 \times 10^{-11} \\ 1.0365 \times 10^{-15} & 576.06 & 2.7882 \times 10^{-3} \\ 5902.8 & 5.5689 \times 10^{-19} & 165900 \end{pmatrix} MeV \quad (4.32)$$

$$\approx \begin{pmatrix} m_u & 0 & 0 \\ 0 & m_c & 0 \\ 0 & 0 & m_t \end{pmatrix}, \quad (4.33)$$

and:

$$\mathbf{m_d} = \begin{pmatrix} 1.6660 \times 10^{-73} & 16.947 & 5.4422 \times 10^{-20} \\ 14.510 & 8.0344 \times 10^{-18} & 123.42 \\ 2.1526 \times 10^{-23} & 1373.2 & 2370.2 \end{pmatrix} MeV \quad (4.34)$$

---

[2]The element $m_{u(1,3)} = 5902.8 MeV$ is negligible because it is in the same row as the much larger top mass, and can be removed by a small 1-3 rotation redefining the U_i^c fields.
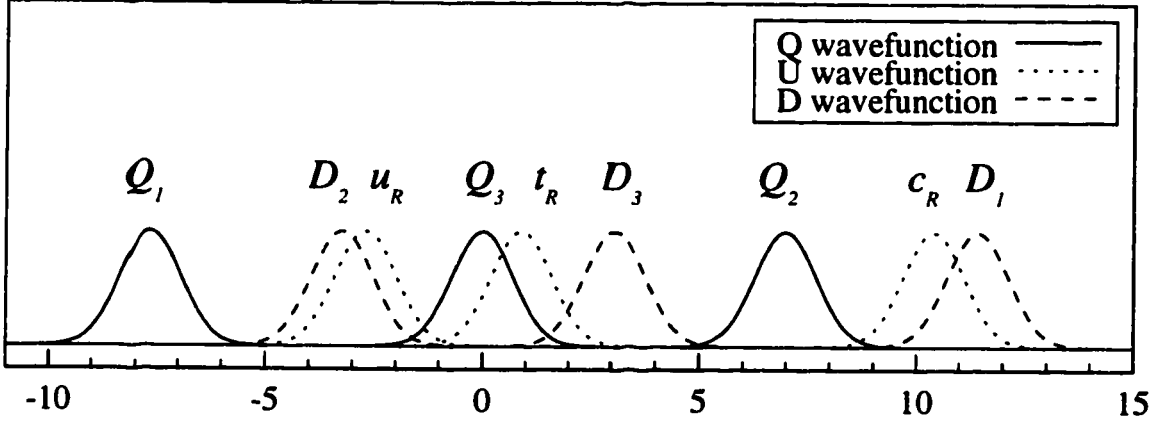
Figure 4.5: The locations of the quark wavefunctions.

$$\approx \begin{pmatrix} 0 & m_s V_{us}/\cos(\theta) & 0 \\ m_d/V_{us} & 0 & m_b V_{cb}/\cos(\theta) \\ 0 & m_b\sin(\theta) & m_b\cos(\theta) \end{pmatrix}. \tag{4.35}$$

which, using equations (4.18) - (4.20) and running using the scaling parameters in the appendix, gives masses:

$$\begin{array}{ll} m_u = 3.24 \ MeV & m_d = 6.01 \ MeV \\ m_c = 1250. \ MeV & m_s = 120 \ MeV \ , \\ m_t = 166000 \ MeV & m_b = 4250 \ MeV \end{array} \tag{4.36}$$

and CKM matrix elements:

$$\mathbf{V_{CKM}} = \begin{pmatrix} 0.9755 & 0.2200 & 0.0031 \\ 0.2197 & 0.9748 & 0.0390 \\ 0.0116 & 0.0373 & 0.9992 \end{pmatrix}, \tag{4.37}$$

which are consistent with experiment. The configuration is depicted graphically in figure 4.5.

The down mass matrix texture of equation (4.35) differs from the example texture of equation (4.28) only by a 2-3 rotation by θ re-defining the D_i^c fields, given that a certain additional relation among the entries holds. The rotation on the D_i^c fields

transforms the down mass matrix from equation (4.35) as:

$$\mathbf{m_d} \rightarrow \mathbf{m_d'} = \begin{pmatrix} 0 & m_s V_{us} & m_s V_{us} \sin(\theta)/\cos(\theta) \\ m_d/V_{us} & m_b V_{cb} \sin(\theta)/\cos(\theta) & m_b V_{cb} \\ 0 & 0 & m_b \end{pmatrix}, \qquad (4.38)$$

which agrees with the texture of equation (4.28) if we can make:

$$m_s V_{us} \sin(\theta)/\cos(\theta) = m_b V_{ub} \qquad (4.39)$$

$$m_b V_{cb} \sin(\theta)/\cos(\theta) = m_s. \qquad (4.40)$$

We can choose θ so that one of the equations is satisfied (for example, we could choose $\tan(\theta) = m_s/(m_b V_{cb})$ to satisfy equation (4.40)). If one equation is satisfied, the other will be as well if the relation:

$$m_b V_{ub}/m_s V_{us} = \sin(\theta)/\cos(\theta) = m_s/m_b V_{cb}, \qquad (4.41)$$

is satisfied. As the mass of the strange quark is the most uncertain of the quantities in equation (4.41), we re-write this relation as:

$$m_s = (V_{ub} V_{cb}/V_{us})^{1/2} \times m_b, \qquad (4.42)$$

which holds at the common scale m_t. Running the masses down to their physical scales using the factors in the appendix gives:

$$m_s^{\overline{MS}}(2 \; GeV) \approx (1.19) \times (V_{ub} V_{cb}/V_{us})^{1/2} \times m_b^{\overline{MS}}(m_b) \approx 120 \; MeV. \qquad (4.43)$$

The relation of equation (4.43) is consistent with experiment, and represents the "prediction" present in this model which allows it to fit nine observables with eight model parameters.

There are also seven other configurations giving the same masses and mixings which result from the fact that, for all three i, moving the U_i^c fields to the opposite side of its partner quark doublet Q_i while keeping their relative distance fixed leaves
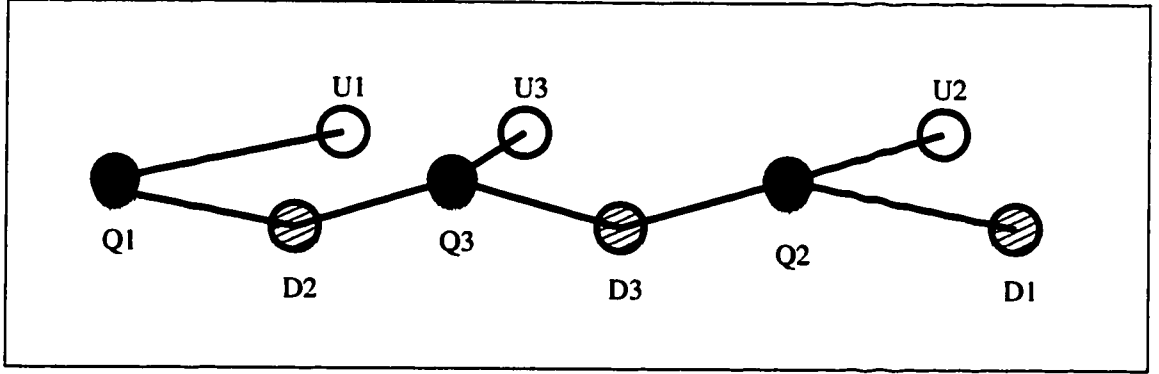
Figure 4.6: The constrained distances between the quark wavefunctions.

the diagonal elements of m_u unchanged while not carrying the U_i^c so close to the other quark doublets $Q_{j\neq i}$ that they create large off-diagonal elements in m_u. These solutions are described by changing the $+$ signs to $-$ signs in equation (4.30). As these other configurations produce the same mass matrices, they yield the same prediction for the strange mass of equation (4.43).

No other such distance preserving re-arrangements to the configuration can be made without bringing otherwise distant fields too close and thus creating large unwanted mass matrix elements which destroy the predictions above. The constrained distances between the wavefunction locations are illustrated in figure 4.6.

4.8 The Complete Landscape

We now present a portrait of the complete wavefunction landscape. The final constraint for including both the lepton and quark wavefunctions together is to separate the leptons and quarks sufficiently to suppress proton decay. The analysis of [47] shows that a separation distance $\approx 10 \times \mu^{-1}$ between the nearest quark and lepton fields is sufficient. Putting together the configurations found in section 4.4 and section
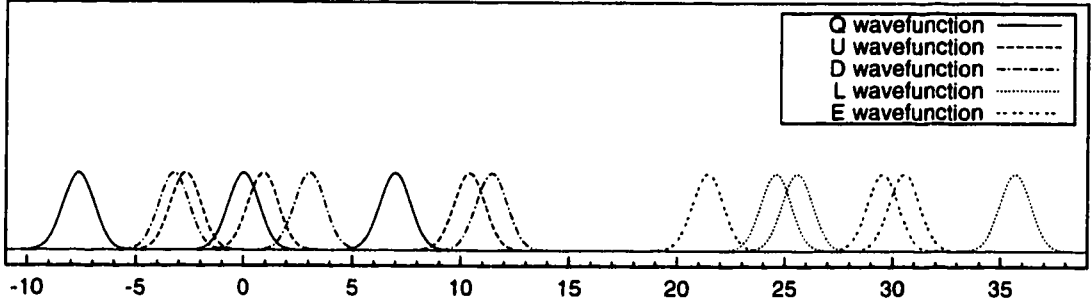
Figure 4.7: The locations of all the wavefunctions.

4.7 gives us one possible configuration:

$$
q_i = \mu^{-1} \begin{pmatrix} -7.6057 \\ 6.9522 \\ 0.0 \end{pmatrix}, \quad u_i = \mu^{-1} \begin{pmatrix} -2.7357 \\ 10.4362 \\ 0.9012 \end{pmatrix}, \quad d_i = \mu^{-1} \begin{pmatrix} 11.3682 \\ -3.2250 \\ 3.0511 \end{pmatrix},
$$

$$
l_i = \mu^{-1} \begin{pmatrix} 35.593 \\ 25.518 \\ 24.5184 \end{pmatrix}, \quad e_i = \mu^{-1} \begin{pmatrix} 30.465 \\ 29.466 \\ 21.368 \end{pmatrix}, \tag{4.44}
$$

which is depicted graphically in figure 4.7. This requires a wall thickness $L \approx 44$ which is just within the boundary of applicability of our treatment as defined by equations (4.10)-(4.13). The analysis in [47] is for a theory with a cut-off scale $M_* \sim 1\ TeV$. Higher cut-off scales allow for smaller lepton-quark separations, and at a scale $M_* \sim 10^{13}\ TeV$ the leptons and quarks do not need to be separated at all.

4.9 Conclusion

It is pleasing to discover that Arkani-Hamed and Schmaltz's solution to the Yukawa hierarchy problem can be made concrete, and that the masses and mixings of the standard model, while highly constraining, do not have any hidden relations that prevent their generation from a configuration of wavefunction displacements. It is also gratifying that the minimal model described contains a prediction which may be

falsified or supported by future experimental data.

4.10 Appendix A:
Derivation of the Zero Mode

In this appendix we demonstrate that a minimal five-dimensional spinor coupled to a scalar field with a generic domain-wall expectation value profile in the fifth dimension leads to a single chiral fermion zero mode localized at the zero crossing of the scalar field. We show that if the scalar profile is linear, the zero mode has a Gaussian profile, with the higher modes having the spectrum and profile associated with harmonic oscillator wave-functions.

The five-dimensional action:

$$S = \int d^5x \ \overline{\Psi}[i\gamma^A \partial_A + \Phi(x_5)]\Psi, \tag{4.45}$$

can be decomposed into four-dimensional terms:

$$S = \int d^4x \int dx_5 \ \overline{\Psi}[i\gamma^\mu \partial_\mu + i\gamma^5 \partial_5 + \Phi(x_5)]\Psi. \tag{4.46}$$

In chiral spinor notation, this is:

$$S = \int d^4x \int dx_5 \ [\psi_L^\dagger \ \ \psi_R^\dagger] \cdot \begin{bmatrix} i\partial_\mu \overline{\sigma}^\mu & -\partial_5 + \Phi(x_5) \\ +\partial_5 + \Phi(x_5) & i\partial_\mu \sigma^\mu \end{bmatrix} \cdot \begin{bmatrix} \psi_L \\ \psi_R \end{bmatrix}. \tag{4.47}$$

We can split the spinors into a 4-dimensional spinor part ψ multiplied by an extra-dimensional profile (with no spin indices) ζ:

$$\Psi(x_m) = \sum_i \begin{bmatrix} \psi_{L(i)}(x_\mu)\zeta_i^L(x_5) \\ \psi_{R(i)}(x_\mu)\zeta_i^R(x_5) \end{bmatrix}, \tag{4.48}$$

and integrate over x_5 to get:

$$S = \int d^4x \psi_{L(0)}^\dagger [i\overline{\sigma}_\mu \partial_\mu] \psi_{L(0)} + \psi_{R(0)}^\dagger [i\sigma_\mu \partial_\mu] \psi_{R(0)}$$

$$+ \sum_i \overline{\Psi}_{(i)}[i\gamma_\mu \partial_\mu - m_i]\Psi_{(i)}, \tag{4.49}$$

where the m_i and $\zeta_i^{L,R}$ are chosen such that:

$$(-\partial_5 + \Phi(x_5))\zeta_i^R(x_5) = m_i \zeta_i^L(x_5) \tag{4.50}$$

$$(+\partial_5 + \Phi(x_5))\zeta_i^L(x_5) = m_i \zeta_i^R(x_5), \tag{4.51}$$

and we have defined:

$$\Psi(x_\mu)_{(i)} = \begin{bmatrix} \psi_{L(i)}(x_\mu) \\ \psi_{R(i)}(x_\mu) \end{bmatrix}. \tag{4.52}$$

From equations (4.50) and (4.51) we find zero modes:

$$(-\partial_5 + \Phi(x_5))\zeta_0^R(x_5) = 0 \tag{4.53}$$

$$(+\partial_5 + \Phi(x_5))\zeta_0^L(x_5) = 0, \tag{4.54}$$

with solutions:

$$\zeta_0^R(x_5) = A_0^R e^{+\int_0^{x_5} \Phi(y_5)dy_5} \tag{4.55}$$

$$\zeta_0^L(x_5) = A_0^L e^{-\int_0^{x_5} \Phi(y_5)dy_5}, \tag{4.56}$$

where the A are normalization constants chosen to make $\int dx^5 \zeta^* \zeta = 1$. In the approximation $\Phi(x_5) = 2\mu^2 x_5$ this is:

$$\zeta_0^R(x_5) = Ae^{+\mu^2 x_5^2} \tag{4.57}$$

$$\zeta_0^L(x_5) = Ae^{-\mu^2 x_5^2}, \tag{4.58}$$

so the left-handed solution $\zeta_0^L(x_5)$ is a Gaussian and the right-handed solution $\zeta_0^R(x_5)$ is non-normalizable—only the left-handed solution is physical. By inspection of equations (4.55) and (4.56) we see that this is a generic feature of any function $\Phi(x_5)$ that goes from a finite negative asymptotic value to a finite positive asymptotic value with one zero crossing. If the Yukawa coupling were multiplied by -1 or if the scalar profile went from positive to negative, the right-handed solution would have been the

physical solution and the left-handed solution would have been non-normalizable.

If the scalar expectation value dipped back through zero, as in a configuration of two domain walls coming from a kink/antikink profile, there would be a mirror zero-energy chiral fermion stuck on the other wall. In the limit that the second domain wall (and its mirror fermion) are infinitely far away, we recover the case discussed above.

To examine the massive spectrum, we operate on equation (4.50) with $(+\partial_5 + \Phi(x_5))$ and equation (4.51) with $(-\partial_5 + \Phi(x_5))$ and use $\Phi(x_5) = 2\mu^2 x_5$ to obtain:

$$(-\partial_5^2 + (2\mu^2 x_5)^2 + 2\mu^2)\zeta_i^R(x_5) = m_i^2 \zeta_i^R(x_5) \tag{4.59}$$

$$(-\partial_5^2 + (2\mu^2 x_5)^2 - 2\mu^2)\zeta_i^L(x_5) = m_i^2 \zeta_i^L(x_5). \tag{4.60}$$

$$\tag{4.61}$$

Recognizing these as harmonic oscillator Schrödinger equations for a particle with mass $\hbar^2/2$, characteristic angular frequency $\omega_0 = 4\mu^2/\hbar$ and ground state energy $\pm 2\mu^2$, we can immediately write down the solution:

$$m_n^2 = 4\mu^2 n \quad (n = 0, 1, 2, 3, ...) \tag{4.62}$$

$$\zeta_n^L(x_5) = \zeta_{n+1}^R(x_5) = (\frac{a^\dagger}{\sqrt{n!}})^n \zeta_0^L(x_5) \equiv \frac{1}{\sqrt{n!}}(\frac{-\partial_5 + 2\mu^2 x_5}{2\mu})^n \zeta_0^L(x_5). \tag{4.63}$$

In this framework we can see the chirality of the zero mode by noting that the ground state energy shift term $\pm 2\mu^2$ of the Schrödinger equation shifts the eigenvalue tower from the usual $\sim 1/2, 3/2, 5/2...$ down to $\sim 0, 1, 2...$ for the left handed modes and up to $\sim 1, 2, 3...$ for the right handed modes.

4.11   Appendix B:
Standard Model Parameters

For the experimentally allowed values of the standard model parameters, we used[49]:

$$m_u = 1.5 \text{ to } 5 \; MeV$$
$$m_d = 3 \text{ to } 9 \; MeV$$
$$m_s = 60 \text{ to } 170 \; MeV$$

$$m_u/m_d = 0.20 \text{ to } 0.70$$
$$(m_u + m_d)/2 = 2 \text{ to } 6 \; MeV$$
$$(m_s - (m_u + m_d)/2)/(m_d - m_u) = 34 \text{ to } 51$$

$$m_c = 1100 \text{ to } 1400 \; MeV$$
$$m_b = 4100 \text{ to } 4400 \; MeV$$
$$m_t = 166000 \pm 5000 \; MeV$$

$$V_{us} = 0.217 \text{ to } 0.224$$
$$V_{ub} = 0.0018 \text{ to } 0.0045$$
$$V_{cb} = 0.036 \text{ to } 0.042$$

$$m_e = 0.5110 \; MeV$$
$$m_\mu = 105.7 MeV$$
$$m_\tau = 1777 \; MeV,$$

$$(4.64)$$

where the quark masses are in the $\overline{MS}$ renormalization scheme. The up, down, and strange masses are evaluated at a scale of 2 GeV, while the other quark masses are

evaluated at a scale equal to their $\overline{MS}$ mass. The lepton masses are pole masses.

To run the quark masses to the common scale m_t, we used the three-loop QCD and one-loop QED scaling factors[50]:

η_u	η_d	η_s	η_c	η_b	η_t
1.84	1.84	1.84	2.17	1.55	1.00

(4.65)

where $\eta_i = m_i(m_i)/m_i(m_t)$ for $i = c, b, t$ and $\eta_i = m_i(2\ GeV)/m_i(m_t)$ for $i = u, d, s$. The lepton pole masses were related to their $\overline{MS}$ masses evaluated at m_t using the relation

$$m^{\text{pole}} = m^{\overline{MS}}(\mu) \left(1 + \frac{\alpha}{\pi} \left[1 + \frac{3}{4}\log(\frac{\mu^2}{m^2}) \right] \right)$$

(4.66)

to give scaling factors

η_e	η_μ	η_τ
1.05	1.03	1.02

(4.67)

where $\eta_i = m_i^{\text{pole}}(m_i)/m_i^{\overline{MS}}(m_t)$.

Bibliography

[1] E. A. Mirabelli and M. E. Peskin, "Transmission of Supersymmetry Breaking From a Four-Dimensional Boundary," Phys. Rev. D **58**, 65002 (1988), hep-th/9712214.

[2] E. A. Mirabelli, M. Perelstein, and M. E. Peskin "Collider Signatures of New Large Space Dimensions," Phys. Rev. Lett. **82**, 2236 (1999), hep-ph/981133.

[3] E. A. Mirabelli and M. Schmaltz, to appear.

[4] Nima Arkani-Hamed, Savas Dimopoulos, John March-Russell, "Stabilization of Submillimeter Dimensions: The New Guise of the Hierarchy Problem" hep-th/9809124.

[5] P. Hořava and E. Witten, "Heterotic and Type I String Dynamics From Eleven-Dimensions," Nucl. Phys. **B460** (1996) 506, 1996, hep-th/9510209.

[6] P. Hořava and E. Witten, "Eleven Dimensional Supergravity on a Manifold With Boundary," Nucl. Phys. **B475** (1996) 94, hep-th/9603142.

[7] E. Witten, "Strong Coupling Expansion of Calabi-Yau Compactification," hep-th/9602070.

[8] P. Hořava, *Phys. Rev.* D **54**, 7561 (1996), hep-th/9608019.

[9] E. Sharpe, hep-th/9611196.

[10] H. G. B. Casimir, *Proc. Kong. Ned. Akad. Wet.* B **51**, 793 (1948).

[11] T. Banks and M. Dine, *Nucl. Phys.*B **479**, 173 (1996), hep-th/9605136.

[12] I. Antoniadis, S. Ferrara, and T. R. Taylor, *Nucl. Phys.* B **460**, 489 (1996), hep-th/9511108.

[13] K. Choi, *Phys. Rev.* D **56**, 6588 (1997), hep-th/9706171.

[14] T.-J. Li, J. L. Lopez, and D. V. Nanopoulos, *Phys. Rev.* D **56**, 2602 (1997), hep-ph/9704247.

[15] H. P. Nilles, M. Olechowski, and M. Yamaguchi, *Phys. Lett.* B **415**, 24 (1997), hep-th/9707143.

[16] Z. Lalak and S. Thomas, hep-th/9707223.

[17] K. Choi, H. B. Kim, and C. Munoz, hep-th/9711158.

[18] A. Lukas, B. A. Ovrut, and D. Waldram, hep-th/9711197.

[19] M. Dine, R. Rohm, N. Seiberg, and E. Witten, *Phys. Lett.* B **156**, 55 (1985).

[20] E. Dudas and C. Grojean, *Nucl. Phys.* B **507**, 553 (1997), hep-th/9704177.

[21] I. Antoniadis and M. Quirós, *Nucl. Phys.* B **505**, 109 (1997), hep-th/9705037; I. Antoniadis and M. Quirós, *Phys. Lett.* B **416**, 327 (1998), hep-th/9707208.

[22] J. Scherk and J. H. Schwarz, *Phys. Lett.* B **82**, 60 (1979).

[23] P. Brax and N. Turok, *Phys. Lett.* B **413**, 331 (1997), hep-th/9706035.

[24] P. West, *Introduction to Supersymmetry and Supergravity*, (World Scientific, Singapore, 1986).

[25] J. Wess and J. Bagger, *Supersymmetry and Supergravity*, (Princeton University Press, Princeton, 1992).

[26] M. Dine, A. E. Nelson, and Y. Shirman, *Phys. Rev.* D **51**, 1362 (1995), hep-ph/9408384;

M. Dine, A. E. Nelson, Y. Nir, and Y. Shirman, *Phys. Rev.* D **53**, 2658 (1996), hep-ph/9507378.

[27] S. Martin, *Phys. Rev.* D **55**, 3177 (1997), hep-ph/9608224.

[28] E. Poppitz and S. P. Trivedi, *Phys. Lett.* B **401**, 38 (1997), hep-ph/9703246.

[29] J. van der Bij and M. Veltman, *Nucl. Phys.* B **231**, 205 (1984).

[30] G. F. Giudice and R. Rattazzi, *Nucl. Phys.* B **511**, 25 (1998), hep-ph/9706540.

[31] S. Dimopoulos, G. F. Giudice, and A. Pomerol, *Phys. Lett.* B**389**, 37 (1996), hep-ph/9607225.

[32] I. Antoniadis, Phys. Lett. B **246**, 377 (1990).

[33] This idea has recently been developed further by J. Lykken, Phys. Rev. D **54**, 3693 (1996), hep-th/9603133, and by K. Dienes, E. Dudas, and T. Ghergetta, Phys. Lett. B **436**, 55 (1998), hep-ph/9803466.

[34] R. Sundrum, hep-ph/9708329.

[35] N. Arkani-Hamed, S. Dimopoulos, and G. Dvali, Phys. Lett. B **429**, 263 (1998), hep-ph/9803315; I. Antoniadis, N. Arkani-Hamed, S. Dimopoulos, and G. Dvali, Phys. Lett. B **436**, 257 (1998), hep-ph/9804398; N. Arkani-Hamed, S. Dimopoulos, and G. Dvali, hep-ph/9807344.

[36] G. Shiu and S.-H. H. Tye, Phys. Rev. D **58**, 106007 (1998), hep-th/9805157; Z. Kakushadze and S.-H. H. Tye, hep-th/9809147.

[37] V. P. Mitrofanov and O. I. Ponomareva, *Sov. Phys. JETP* **67**, 1963 (1988).

[38] Macroscopic bounds on modifications of gravity have recently been reviewed by J. C. Long, H. W. Chan, and J. C. Price, hep-ph/9805217.

[39] The generality of this result is explained carefully in R. Sundrum, hep-ph/9805471.

[40] T. Stelzer and W.F. Long, Comput. Phys. Commun. **81**, 357 (1994), hep-ph/9401258.

[41] F. A. Berends, G. J. H. Burgers, C. Mana, M. Martinez, and W. L. van Neerven, Nucl. Phys. B **301**, 583 (1988).

[42] R. Barate, *et al.* (ALEPH Collaboraton), Phys. Lett. B **429**, 201 (1998); M. Acciarri, *et al.* (L3 Collaboration), Phys. Lett. B **444**, 503 (1998); G. Abbiendi, *et al.* (OPAL Collaboration), hep-ex/9810021.

[43] R. Markeloff (CDF Collaboration), in *The Fermilab Meeting, DPF '92*, C. H. Albright, P. H. Kasper, R. Raja, and J. Yoh, eds. (World Scientific, Singapore, 1993); R. Markeloff, University of Wisconsin Ph. D. thesis, 1992.

[44] Later publications from the CDF and D0 experiments on searches for missing E_T have required in addition the presence of at least 3 jets; see, for example M. Chertok, FERMILAB-Conf-98/156-E, to appear in the *Proceedings of the 33rd Rencontres de Moriond: QCD and High Energy Hadronic Interactions*, J. Tran Thanh Van, ed.

[45] H. L. Lai, *et al.* (CTEQ Collaboration), Phys. Rev. D **55**, 1280 (1997), hep-ph/9606399.

[46] T. Han, J.D. Lykken and R. Zhang, hep-ph/9811350; J. L. Hewett,hep-ph/9811356; P. Mathews, S. Raychaudhuri and K. Sridhar, hep-ph/9812486; T. G. Rizzo, hep-ph/9901209, G. F. Giudice, R. Rattazzi, and J. D. Wells, hep-ph/9811291.

[47] Nima Arkani-Hamed and Martin Schmaltz, "Hierarchies Without Symmetries From Extra Dimensions", hep-ph/9903417.

[48] M. E. Peskin and D. V. Schroeder, *An Introduction to Quantum Field Theory.* (Addison-Wesley, Menlo Park, 1995).

[49] C. Caso et. al., Eur. Phys. J. C **3**, 1 (1998).

[50] V. Barger, M.S. Berger, T. Han and M. Zralek, Phys. Rev. Lett. **68**, 3394 (1992), hep-ph/9203220.

G. W. Anderson, S. Raby, S. Dimopoulos, L. J. Hall, Phys. Rev. D **47**, 3702 (1993), hep-ph/9209250.

K. Babu and R. Mohapatra, Phys. Rev. Lett. **74**, 2418 (1995).

H. Fusaoka, Y. Koide, hep-ph/9706211.

[51] W. H. Press, S. A. Teukolsky, W. T. Vetterling and B. P. Flannery, *Numerical Recipes in C, Second Edition.* (Cambridge University Press, Cambridge, 1992).